A unified Planar Poisson's Ratio Design Method (PPRDM) for meiotic metamaterials that exhibit negative compressibility based on a minimal chiral meiotic structure

Roberjot, Pierre; Herder, Just L.

DOI
10.1016/j.ijsolstr.2025.113494

Publication date
2025

Document Version
Final published version

Published in
International Journal of Solids and Structures

Citation (APA)
Roberjot, P., & Herder, J. L. (2025). A unified Planar Poisson's Ratio Design Method (PPRDM) for meiotic metamaterials that exhibit negative compressibility based on a minimal chiral meiotic structure. *International Journal of Solids and Structures*, *320*, Article 113494. https://doi.org/10.1016/j.ijsolstr.2025.113494

International Journal of Solids and Structures 320 (2025) 113494

Contents lists available at ScienceDirect

International Journal of Solids and Structures

journal homepage: www.elsevier.com/locate/ijsolstr

A unified Planar Poisson's Ratio Design Method (PPRDM) for meiotic metamaterials that exhibit negative compressibility based on a minimal chiral meiotic structure

Pierre Roberjot *, Just L. Herder

Delft University of Technology, Department of Precision and Microsystems Engineering, Mekelweg 2, 2628CD, Delft, The Netherlands

ARTICLE INFO

Keywords:
Meiotic
Auxetic
Metamaterials
Poisson's ratio
Rational design
Negative linear compressibility

ABSTRACT

Meiotic metamaterials are intricately designed structures characterized by a positive Poisson's ratio, surpassing the conventional limit of 0.5 observed in natural materials. This exceptional attribute allows them to contract or expand perpendicularly to the applied stretch or compression, respectively.

Structures featuring a high positive Poisson's ratio exhibit a counter-intuitive negative compressibility behavior, holding significant promise for diverse applications spanning various domains.

Despite the potential of Poisson's ratio metamaterials, including auxetic, anepirretic, and meiotic structures, their recent development has been hindered by the lack of efficient design methods. This paper aims to address this limitation, concentrating on the meiotic variant of a minimal 2D auxetic structure recently proposed. We employ a design method incorporating two topological transformations, not only enabling the creation of known meiotic structures but also facilitating the generation of new ones while understanding the impact of chirality. Additionally, the proposed method enables the categorization of these structures into three achiral families that present meiotic behavior and can exhibit negative linear compressibility and three chiral families that possess an auxetic behavior. Only the base chiral structure was found to exhibit a meiotic behavior while being chiral.

In an effort to enhance comprehension and standardization, we introduce a naming protocol and define the associated unit cell for these structures. We also delve into the potential of tessellations within this framework. Finally, our study examines meiotic structures from the perspective of surface strain, a more general metrics, linked to the compressibility, providing further insights into their unique mechanical properties.

1. Introduction

In recent decades, a novel category of material mechanisms has emerged, known as metamaterials or metastructures. Metamaterials are architecturally designed structures that showcase unique behaviors, possessing properties unattainable by natural materials. These structures are tessellated and consist of repeating unit cells that enclose an architectured mechanism. One specific type of metamaterial is the Poisson's ratio metastructure, engineered to exhibit specific values and behavior of Poisson's ratio. Typically, isotropic materials have a Poisson's ratio within the range of −1 to 0.5, whereas metamaterials are usually designed to exhibit positive or negative values outside of this natural range. Based on this, three distinct groups can be identified. Firstly, auxetic structures (Kolken and Zadpoor, 2017; Li et al., 2019), are the most common. They possess a negative Poisson's ratio, meaning they expand or compress in the direction opposite to the applied stretch or compression, respectively. Some rare natural materials, such as certain tendons (Gatt et al., 2015b) and bones (Williams and Lewis, 1982), exhibit auxetic behavior. While most auxetic structures have a Poisson's ratio between −1 and 0, certain structures have been observed to surpass the isotropic lower limit of −1 (Dirrenberger et al., 2011; Shaat and Wagih, 2020). The second group comprises anepirretic structures (Dagdelen et al., 2017; Hamzehei et al., 2022). These structures possess a zero Poisson's ratio, maintaining their thickness when subjected to stretching or compression. Cork has been considered to exhibit an almost anepirretic behavior (Fortes and Teresa Nogueira, 1989), with very low Poisson's ratio values in the radial directions ($\nu = 0.067$). The third group is represented by meiotic structures (Dagdelen et al., 2017), characterized by a positive Poisson's ratio. Most natural *materials* exhibit a positive Poisson's ratio, such as rubber ($\nu \approx 0.499$), copper ($\nu = 0.330$), and steel ($\nu = 0.285$). Only rare natural

* Corresponding author.
E-mail addresses: P.Roberjot@tudelft.nl (P. Roberjot), J.L.Herder@tudelft.nl (J.L. Herder).

https://doi.org/10.1016/j.ijsolstr.2025.113494
Received 28 October 2024; Received in revised form 21 May 2025; Accepted 29 May 2025
Available online 23 June 2025

structures exhibit a Poisson's ratio higher than 0.5, for instance the skin of certain aquatic salamanders which possess a Poisson's ratio higher than 2.5 (Frolich et al., 1994). Values as high as 2 where found for symmetrical graphite fiber/epoxy angled ply composites (Chamis, 1980). Meiotic metamaterials are less commonly developed compared to the auxetic, but certain proposals, like those based on the inversor linkage, aim to achieve a constant Poisson's ratio of 1 (Broeren et al., 2019). Notably, well-known pantograph structures also align with the meiotic definition (dell'Isola et al., 2015; Turco et al., 2016; Turco and Rizzi, 2016; dell'Isola et al., 2019).

In 1985, auxetic metamaterials were initially discovered in specific foams (Kolpakov, 1985; Lakes, 1987). Since then, these structures have undergone various modifications, leading to the identification of new auxetic forms. The growing interest in auxetic metamaterials stems from their diverse applications, yet their development has often relied on trial and error. While many structures have been created through this approach, there has been a shift towards more deliberate engineering methods. Some specific design approaches have been proposed to actively craft particular groups of auxetic structures (Grima et al., 2005; Broeren et al., 2019). Auxetic metamaterials can be broadly categorized based on chirality, including chiral (Zhang et al., 2022; Zhu et al., 2022) and achiral (or non-chiral) (Grima et al., 2005; Papadopoulou et al., 2017) structures. Recently (Roberjot and Herder, 2024) proposed a Planar Poisson's Ratio Design Method (PPRDM) based on a structural minimal auxetic unit, serving as a foundational element for planar auxetic metamaterials. The chiral three-beam structure, derived from this minimal unit, has demonstrated auxetic behavior up to a maximum strain. Interestingly, when this structure is extended further, its behavior becomes meiotic. The PPRDM employed holds significant potential for shaping the emerging domain of planar meiotic metamaterials.

The isothermal volume compressibility β_V and the bulk modulus K, its inverse, are two properties that describe how the volume changes in a material when submitted to hydrostatic pressure. Most materials contract in all direction when submitted to hydrostatic pressure, however, constrained structures that express negative compressibility exist and were proven not to violate classical thermodynamics (Grima et al., 2008; Lakes and Wojciechowski, 2008). Negative linear compressibility (NLC) defines the ability of a material or structure to expand in at least one direction when subjected to hydrostatic pressure (Baughman et al., 1998). Such properties have been observed in borate crystal (Kang et al., 2015), zinc dicyanoaurate (Cairns et al., 2013), sodium amidoborane (Magos-Palasyuk et al., 2016), and in some metal–organic framework materials (Wang et al., 2016) under increasing pressure. Materials with a Poisson's ratio below 0.5 possess a positive compressibility whereas a zero compressibility is achieved through a Poisson's ratio of 0.5. Following this idea, metamaterials with a Poisson's ratio above 0.5 would possess a negative compressibility. Such developments have been proposed for planar metamaterials with single material (Baughman et al., 1998; Lakes and Wojciechowski, 2008) and even with multi-material metamaterials (Grima et al., 2008; Gatt and Grima, 2008). Such structures are of interest for potential sensors (Baughman et al., 1998), actuators, and force amplifiers (Nicolaou and Motter, 2012) applications.

Despite their promising potential, the lack of a complete and efficient design method for meiotic metamaterials has hindered their development and widespread applications. Currently, trial-and-error methods are often used to develop these metamaterials, resulting in time-consuming lasting development processes while preventing the creation of general organic classifications.

In this paper, we present an extension of the existing PPRDM to a structural and topological design method for both known and novel 2D meiotic metamaterials formed from a simple minimal meiotic structure. Our three-step design method uses two topological transformations and, creates three achiral and three chiral 2D meiotic families. We first define the topology and strain behavior of the proposed minimal chiral meiotic structure and demonstrate how to create base achiral meiotic structures. Next, we use the design method to create the six meiotic groups, including higher order geometrical structures. We also propose a definition of the unit cells and their tessellations, along with a naming process that encodes the generation process and unit cell type. Then, we suggest characterizing the meiotic structures with surface strain, a more general metric that directly links to the compressibility and shows that negative linear compressibility can be obtain for certain designs.

2. Methods

In this section, we present a minimal chiral meiotic structure derived from the auxetic base structure proposed in Roberjot and Herder (2024) along the auxetic PPRDM. Additionally, we propose three base achiral meiotic structures achieved through the achiralisation of the chiral base. Next, we put forward a unified equation for calculating the Poisson's ratio, which is dependent on the angle of the structures. This equation establishes a link between the auxetic and meiotic base structures. Subsequently, we adapt the design protocol used for 2D auxetic metamaterials to the meiotic base structure. This adaptation allows us to create and categorize meiotic structures into six families, which can be either chiral or achiral. We use a similar naming protocol to encode the geometrical transformations applied to the base structure.

2.1. A minimal chiral meiotic structure emerging from the auxetic base structure

Previously, we proposed a minimal 2D auxetic structure shaped as a "Z" along with a design method that creates six families of planar auxetic metamaterials, a naming protocol and, a unit cell design protocol. The auxetic structure Z_A is a three-bar linkage possessing three rigid beams ($[A'A] = a_1$, $[AB] = a_2$ and $[BB'] = a_3$) linked together with two revolute joints (at points A and B), represented in Fig. 1.a. (for sake of simplicity the revolute joints and sliders are presented here in Fig. 1 and omitted in the rest of the development). It possesses two edges, the points $A' = E_1$ and $B' = E_2$, these points are connection points to tile adjacent Z structures in a line. The regular chiral auxetic Z (Z_A) possesses two acute angles ($\theta_1 = \widehat{A'AB}$ and $\theta_2 = \widehat{ABB'}$, which are equal when Z_A is regular) between 0° and a maximum angle θ_{max} which gives the maximum value of auxeticity, in other words the height of Z is maximum at the angle θ_{max}, illustrated in Fig. 1.b.

The base structure Z_A can be stretched from an initial state where $\theta \leq \theta_{max}$ to a final state where $\theta > \theta_{max}$. In this configuration, any stretch applied to the Z structure will increase the overall length and reduce the height, and therefore, the Poisson's ratio (ν) becomes positive. The configuration where $180° > \theta > \theta_{max}$ gives an overall meiotic behavior, the structure Z is denoted Z_M, and represented in Fig. 1.c.

Z_A and Z_M are topologically equivalent and are considered regular when the length a_1 and a_3 are equals as for the angles θ_1 and θ_2. The unit cell of Z (equivalent for Z_A and Z_M), depicted in Fig. 1.a, b, c, is a rectangular unit cell, the points $E_1 = A'$ and $E_2 = B'$ are the center of two sides of the UC, these sides are normal to the line (E_1O) (or (E_2O)). the two other sides are normal to the two first sides and are passing respectively by the point A and B.

We propose to determine the behavior of the Poisson's ratio ν of the Z structures as a function of the angle θ, for $\theta \in [0°, 180°]$. We assume here a regular Z structure, it possesses a point of symmetry O, and therefore the analysis can be simplified and performed on half of the structures only, as shown and parameterized in Fig. 1.c. The half structures are, for any value of θ, random triangles, thus the Al-Kashi formula can be used to calculate the half-length $L_2 = [E_1O]$ as

$$L_2^2 = a_1^2 + \left(\frac{a_2}{2}\right)^2 - 2a_1\frac{a_2}{2}cos(\theta) \tag{1}$$

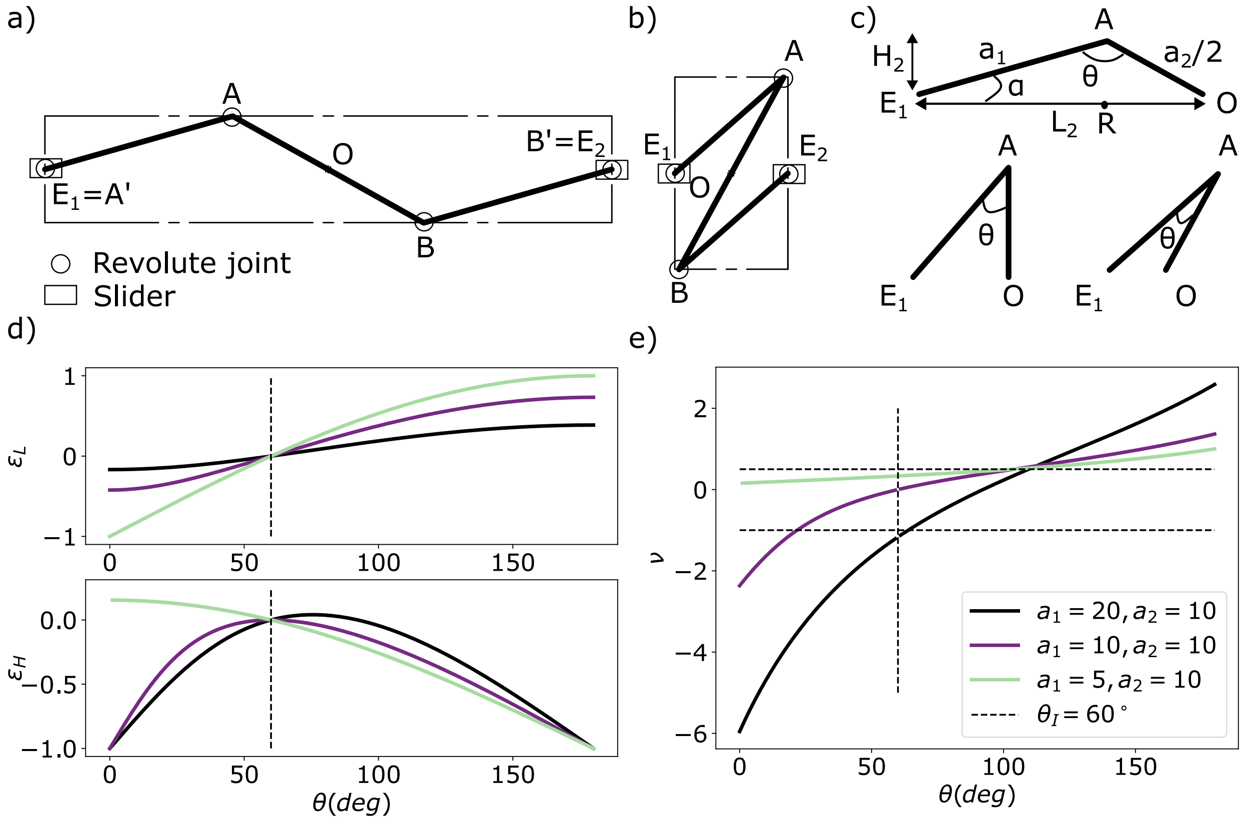

Fig. 1. Representation of the unit cell of (a) Z_M and (b) Z_A with their characteristic points, (c) the parameters of Z, being meiotic, auxetic and at the maximum height, to calculate the half-length L_2 and half-height H_2. Representation of the evolution of the (d) longitudinal ε_L and transverse ε_H strain, and (e) the evolution of the Poisson's ratio ν, with an initial angle $\theta_I = 60°$ for three couples $[a_1, a_2]$. The two horizontal dashed lines represent the isotropic limit of the Poisson's ratio, i.e. $]-1, 0.5[$.

with a_1 the length of the segment $[E_1A]$, $\frac{a_2}{2}$ the length of the segment $[AO]$. The length $L(\theta)$ can be written, as a function of the angle θ, for a couple $[a_1, a_2]$ as,

$$L(\theta) = 2L_2 = 2\sqrt{a_1^2 + \left(\frac{a_2}{2}\right)^2 - 2a_1\frac{a_2}{2}cos(\theta)} \tag{2}$$

The length being known at any angle, the strains $\varepsilon_L(\theta)$ can be calculated as a function of the angle,

$$\varepsilon_L(\theta) = \frac{L(\theta)}{L(\theta_I)} - 1 \tag{3}$$

with θ_I the initial and θ a final angles which give the initial and final length. The strain $\varepsilon_L(\theta)$ is plotted in Fig. 1.d with an arbitrary initial angle $\theta_I = 60°$ for three sets of values of $[a_1, a_2]$. One may notice that the curve $\varepsilon_L(\theta)$ is always growing in the range $[0°, 180°]$ and going from negative values before θ_I to positive values after θ_I.

The height of the UC can be derived similarly, calculating the half-height H_2, which correspond to the projection of the length $[AO]$ on the y axis. The values a_1, $\frac{a_2}{2}$ and $L_2 = \frac{L}{2}$ are known for every θ, thus the law of sines can be applied in the random triangle E_1AO as

$$\frac{L/2}{sin(\theta)} = \frac{a_2/2}{sin(\alpha)} \tag{4}$$

with α the angle $\widehat{AE_1O}$. The value of $sin(\alpha)$ is thus

$$sin(\alpha) = \left(\frac{a_2}{L}\right) sin(\theta) \tag{5}$$

One can form the right triangle E_1AR with R the projection of the point A on the segment $[E_1O]$, where the length of $[AR]$ is the half-height H_2, calculated with the trigonometry as

$$H_2 = a_1 sin(\alpha) \tag{6}$$

or, as a function of θ if Eq. (5) is injected in Eq. (6), as,

$$H(\theta) = 2\frac{a_1a_2}{L(\theta)}sin(\theta) \tag{7}$$

The strain $\varepsilon_H(\theta)$ is given as

$$\varepsilon_H(\theta) = \frac{H(\theta)}{H(\theta_I)} - 1 \tag{8}$$

The evolution of $\varepsilon_H(\theta)$ is plotted in Fig. 1.d. One may notice that the curve $\varepsilon_H(\theta)$ is reaching a growing up to a maximum and then decreasing. Because of the presence of this maximum and the change of sign of $\varepsilon_H(\theta)$ the Poisson's ratio can be either negative or positive.

The Poisson's ratio $\nu(\theta)$ is calculated, as a function of θ from the two strains calculated above,

$$\nu(\theta) = -\frac{\varepsilon_H(\theta)}{\varepsilon_L(\theta)} \tag{9}$$

and plotted in Fig. 1.e with an arbitrary initial angle $\theta_I = 60°$ for three sets of values of $[a_1, a_2]$. One can observe that, with these chosen sets $[a_1, a_2]$ the Poisson's ratio can go down to −6 and up to 2, choosing the dimension of the Z structure directly links to tuning the obtainable strains and PR. In Appendix A we are showing that ν can possess high negative and positive values ($\nu \in [-400, 100]$) depending on the dimension of the beams and the value of the angle, here with $a_1 = 10$ and $a_2 = 0.1$ (arbitrary units). Certain sensing or actuation technologies could benefit from such uncommon values of the Poisson's ratio.

We have shown that, the Poisson's ratio is defined for a given geometry by the angle θ, and since the Z can be auxetic or meiotic, one can define the transition angle θ_T as the angle that separates the auxetic and meiotic topologies. $\theta = \theta_T$ when the triangle E_1AO is a right triangle in O, meaning that $\widehat{E_1OA} = 90°$, therefore, the cosine of $\theta_T = \widehat{E_1AO}$ is calculated as the usual cosine for right triangles

$$cos(\theta_T) = \frac{AO}{AE_1} = \frac{a_2}{2a_1} \tag{10}$$

This angle corresponds to the maximum value of the height $H(\theta)$. The equations derived above hold true for all couples $[a_1, a_2] \in (\Re^*)^2$,

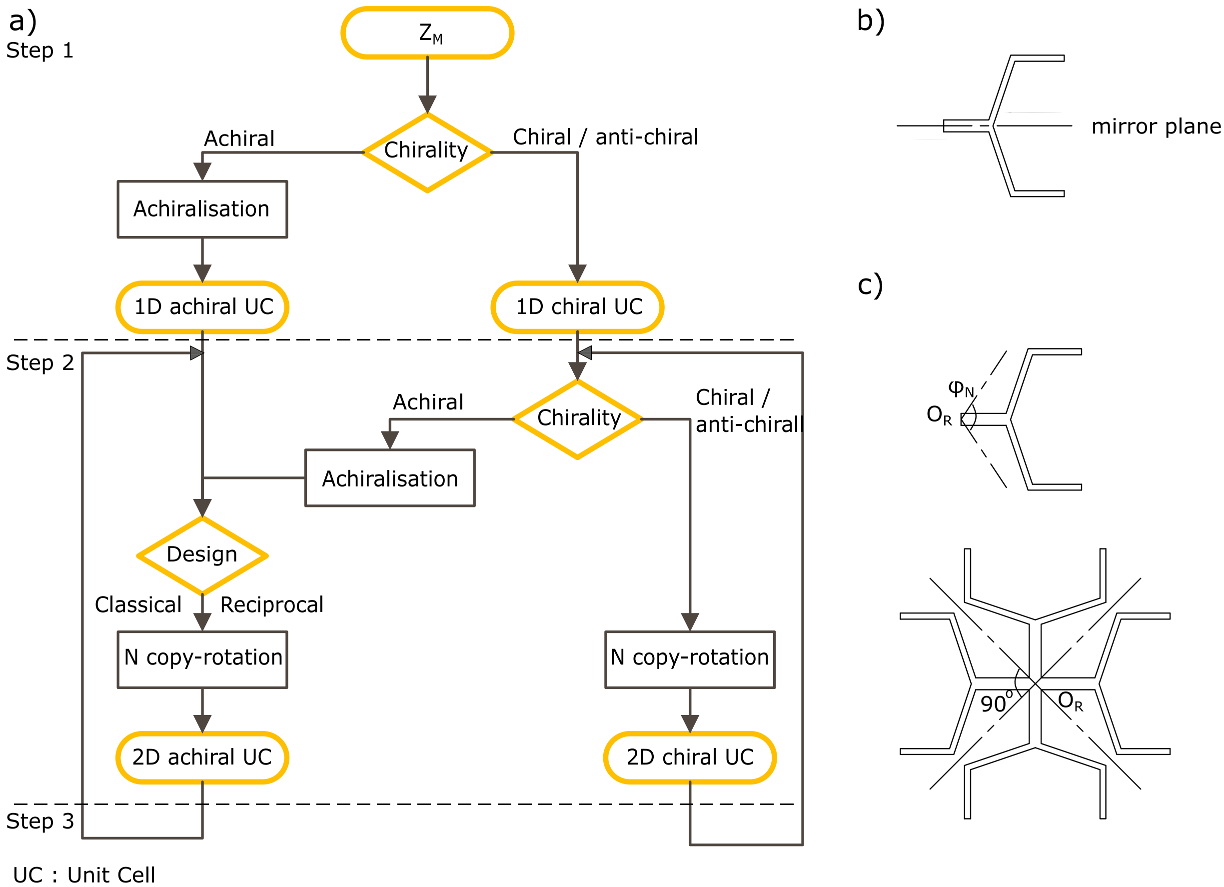

Fig. 2. Representation of (a) the design method applied to the planar auxetic and meiotic metamaterials, with (b) an illustration of the achiralisation process applied to Z_M and, (c) an illustration of the copy rotation of the "Lucky bone" reciprocal design, copy-rotated four times.

however, with the condition that $a_1 \geq a_2/2$. Indeed, if $a_1 > a_2/2$ then the $cos(\theta_T)$ exists and the Z can be either auxetic or meiotic. In the case that $a_1 = a_2/2$, the $cos(\theta_T) = 1$, thus the transition angle $\theta_T = 0$. In this scenario, the structure can only be meiotic.

In the case where $a_1 < a_2/2$, θ_T is not defined, the structure must then be only meiotic. However, if such a structure ($[a_1, a_2]$) is connected to a next one then one can notice that the structure is equivalent to a new Z topology ($[a_1', a_2']$) with $a_1' = a_2/2$ and $a_2' = 2a_1$. In other words, having a Z structure with $a_1 < a_2/2$ is topologically equivalent to having a structure Z' with $a_1 > a_2/2$.

2.2. Design method, classification, naming and tessellation of Z_M-based planar metamaterials

We have been showing that the auxetic structure Z_A can be modified in Z_M to present a meiotic behavior. We are proposing the application of the PPRDM method to the meiotic base structure Z_M. The PPRDM (Fig. 2.a) is a three step method that was presented in Roberjot and Herder (2024), and uses two topological transformations namely "achiralisation" (Fig. 2.b) and "copy-rotation" (Fig. 2.c), the first enables to transform a chiral object in an achiral object using a mirror symmetry, the second displays N copies of an object around a center of rotation O_R.

One rule of transformation is added here to enable the generation of novel designs and variations, When the achiralisation axis is normal to the beam, the edges A' and B' are joined rigidly, however if the axis is of achiralisation is not normal to the beams then the points A' and B' are linked by a revolute joint.

The design method enables to classify the structures in two categories, achiral and chiral structures and six main families. Achiral structures are presented in Section 3.1, three families exist can present a meiotic or anepirretic behavior. Chiral structures originated from Z_M present only an auxetic behavior because they have the same topology of their auxetic counterparts, presented in Section 3.2. When achiralised under certain condition, they may present a meiotic behavior this phenomenon is presented in Section 3.4.2.

The PPRDM could produce an infinite number of structures, therefore a naming protocol is used to encode the topology, chirality, transformations applied to the base structure Z_M and location of the axis of achiralisation and center of rotations (Fig. 3). The naming convention is similar to the auxetic PPRDM coding, and where the base is coded Z_M, the six main families are named and coded similarly. The achiral families are the Lucky bone (Lb) (Cf. Section 3.1.2), the Rose (Ro) (Cf. Section 3.1.3), and the Wine rack (Wr) (Cf. Section 3.1.4). The chiral families are the Missing rib meiotic (Mrm) (Cf. Section 3.2.1), the Closed geometry meiotic (Cgm) (Cf. Section 3.2.2), and the Honeycomb meiotic (Hcm) (Cf. Section 3.2.3). As the chiral families possess the same topology whether built from Z_A or Z_M they have the same base name and added a 'm' when designed with Z_M.

The naming rules are the same as for the auxetic PPRDM, the chiral copy-rotations are written on the right side of the chiral name and separated by a dot "." for higher-order copy-rotations. The achiral transformations are written on the left side with an "A" for the achiralisation, and the type of transformation reciprocal "R" or classical "C", and the number of copy-rotation are written on the left and separated by a dot ".".

The design method produces structures that can be tessellated in the plane (Kolken and Zadpoor, 2017; Czajkowski et al., 2022) to form metastructures. The metastructures are defined with the internal mechanism, the structure, and the contour of the element, the unit cell (UC).

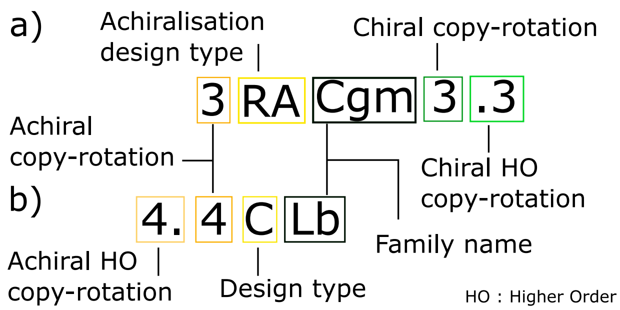

Fig. 3. Details and signification of the naming code with the example of (a) a chiral base structure $3RACgm3.3$, and (b) an achiral base structure $4.4CLb$.

The shape of the unit cell is linked to the number of copy-rotations applied to the base structure and follows the Voronoi decomposition, which creates primitive cells. A structure created after N copy-rotations will possess a UC in the shape of a N-order polygon, as illustrated in Fig. 4. The design process, presented with the auxetic PPRDM, links the edges E_N of the structure to the middle of the N faces F_N of the UC and where the center O_R is the vertex of the cell.

The planar tessellation of the unit cells are following the Archimedean tiling definitions, presented in Appendix B.

3. Results - Application of the design method

In this section we propose to illustrate how the design method can be applied to Z_M to, firstly, design the three achiral base metamaterials following the first step of the design method (Section 3.1.1). Second, we illustrated the second step of the design method, presenting three achiral (Section 3.1) and three chiral (Section 3.2) planar meiotic families, showing the construction of the center of rotation O_R and the edges E_N. Third, we show how higher order (Section 3.3) structures can be generated. We explain that Z_M is a chiral structure that possess a positive Poisson's ratio, however, if used to create chiral structures based on the design method, does generate structures that possess a negative Poisson's ratio, unless the created structures are achiralised in the higher-order. Then, we calculate the Poisson's ratio of some structures to identify ranges of values (Section 3.4).

3.1. Building achiral structures

Here we present three families of achiral meiotic structures originating from Z_M, we illustrate how to create the axis of symmetry for the achiralisation process and the position of the center of rotation O_R. In addition, we detail certain irregular cases that are presented in appendices.

3.1.1. Construction of the achiral meiotic bases

Z_M is, as Z_A is a chiral structure, therefore possesses two enantiomorphs that are the mirror images of each other (Fig. 5.a). The two enantiomorphs can be joined together to form an achiral structure. Joining the enantiomorphs corresponds with placing an axis of symmetry in a particular location and using the axis as a mirror to Z_M, we present here three remarkable axes of achiralisation that allow to built the achiral bases. These three axes are remarkable because they are enable creating known structures, and are following natural symmetries (for instance an x or y axis symmetry).

The first achiralisation, designed as "Lucky bone" (Fig. 5.b), is mirroring Z from the line $(A'A)$ or $(B'B)$. It generates one half of the hexagonal honeycomb structure (Grima et al., 2011). The structure is fully deployed when the angles θ are minimum $\theta_{max} = 0°$ and undeployed when $\theta = 90°$ (in the meiotic regime). The family of the Lb structure is presented in Section 3.1.2.

The second, designed as "Rose" design (Fig. 5.c), is mirroring Z_M from a line normal to $(A'A)$ passing by the point A' (or normal to $(B'B)$ and passing by B'). It generates also one half of the hexagonal honeycomb structure. The structure is fully deployed when the angles θ are minimum $\theta_{max} = 0°$ and undeployed when $\theta = 90°$. The family of the Ro structure is presented in Section 3.1.3.

The third achiralisation, called "Wine racks" (Grima et al., 2008), is mirroring Z_M from the line $(A'B')$, this results in creating a structure that in composed of two lozenges possessing revolute joints at the points O, A_1, A_2, A', B_1, B_2, and B', making a slight exception to the second rule (Section 2.2). The topology and kinematics are represented in Fig. 5.d, the family of Wr is presented in Section 3.1.4.

3.1.2. Achiral "lucky bone" (Lb) design

Here we show how to use the copy-rotation on the three achiral base structures and how to define the center of rotation O_R and the edges E to design the achiral classical and reciprocal structures, illustrated for $N = 2, 3$ and 4. We show how the most common achiral meiotic structures are designed and how an anepirretic structure is created.

Meiotic achiral "Lucky bone" structures, coded Lb, originates from Z_M achiralised as shown in Fig. 5.d. The Fig. 6.a shows the points of interest and the creation of the center of rotation O_R for the classical structures CLb. The point O_R is created from the isosceles triangle $A_1O_RA_2$, with φ_N the angle $\widehat{A_1O_RA_2}$, the edge E of a sector is located at the point B'. The beams A_1A_1' and A_2A_2' need to be removed (or have a length of 0) for the creation of CLb, this choice is made considering their auxetic counterpart, if the beams are present in the structures, it increases the number of moving beams (increasing the number of degrees of freedom) and increasing the number of internal degree of freedom and, thus it is more difficult to control their behavior.

The N copy-rotated structures are linked around O_R connecting the points A_{1n} to the points $A_{2(n+1)}$. The classical case $2CLb$, depicted in Fig. 6.c, has been proposed and named hexagonal honeycomb (Grima et al., 2011) as a variation of the auxetic bow tie structure (Kolken and Zadpoor, 2017). Whereas for the auxetic design, all of the copy-rotated sectors were behaving in the same way, the deformation of meiotic structures is symmetric regarding the axis of stretch, the joint beams between two copy-rotated structures are conserving the same angle and the sectors are getting thinner if on the stretch line or wider if not. The design $4CLb$ is topologically close to one of the proposed topologically optimized Missing-rib structure (Clausen et al., 2015) exhibiting a Poisson's ratio of 0.8. The design method is giving a topological explanation of the high positive Poisson's ratio.

Reciprocal designs of the achiral lucky bone (RLb) are created from the triangle $A_1B'A_2$ (Fig. 6.f), the center of rotation O_R becomes the point B'. The beams A_1A_1' and A_2A_2' are no longer sacrificial beams for these structures. The two edges of the structure are thus the points $E_1 = A_1'$ and $E_2 = A_2'$. The copy-rotation angle φ_N is created between consecutive repetitions of the element, meaning $\varphi_N = \widehat{B_nB'B_{n+1}}$, with B_n and B_{n+1} the points B in the consecutive copy-rotated structures. The reciprocal designs, starting from $N = 3$, possess a decoupling cross-like rigid body at the center of the structure (Fig. 6.h.i), therefore, if a reciprocal structure is stretched in one direction, only the sectors in the line of stretch are subject to deformation. This behavior gives to reciprocal lucky bone structures an anepirretic, or zero Poisson's ratio property (Dagdelen et al., 2017), as would its auxetic counterpart do (Roberjot and Herder, 2024). Anepirretic structures can be built from structures possessing a decoupling link, that links an even number of copy-rotated structures.

3.1.3. Achiral "Rose" (Ro) design

Meiotic "Rose" structures, coded Ro, are built from Z_M achiralised as shown in Fig. 5.e. The center of rotation for the classical Rose design is created from the isosceles triangle $A_1O_RA_2$, φ_N is the angle $\widehat{A_1O_RA_2}$, and the edge point E is located at the point $B_1' = B_2'$ (Fig. 7.a). The N copy-rotated structures are linked around O_R connecting the points

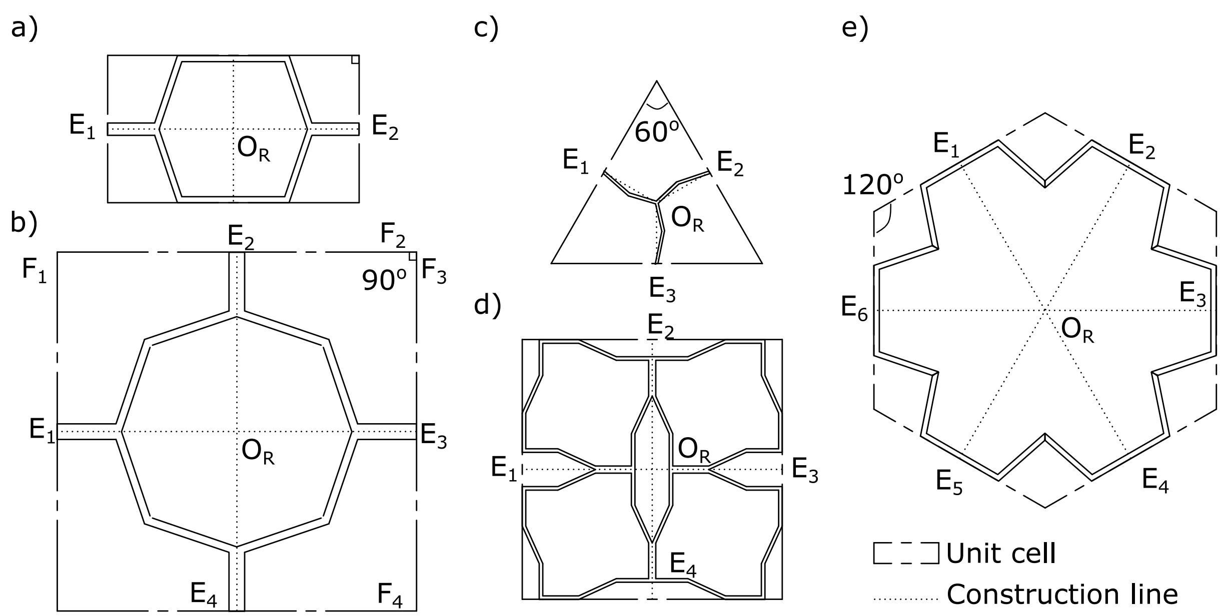

Fig. 4. Representation of the unit cell with the construction lines and center of rotation O_R of (a) $2CLb$ with the four edge points $E_1 - E_4$, (b) $4CLb$ with the four faces F, the four edge points, and the angle $\varphi_3 = 90°$, (c) the triangular UC of $Mrm3$ with the angle $\varphi_3 = 60°$, (d) the example of $2CACgm4$ an higher order structure, and (e) the hexagonal UC of $6CRo$ with the six edges $E_1 - E_6$ and the angle $\varphi_6 = 120°$.

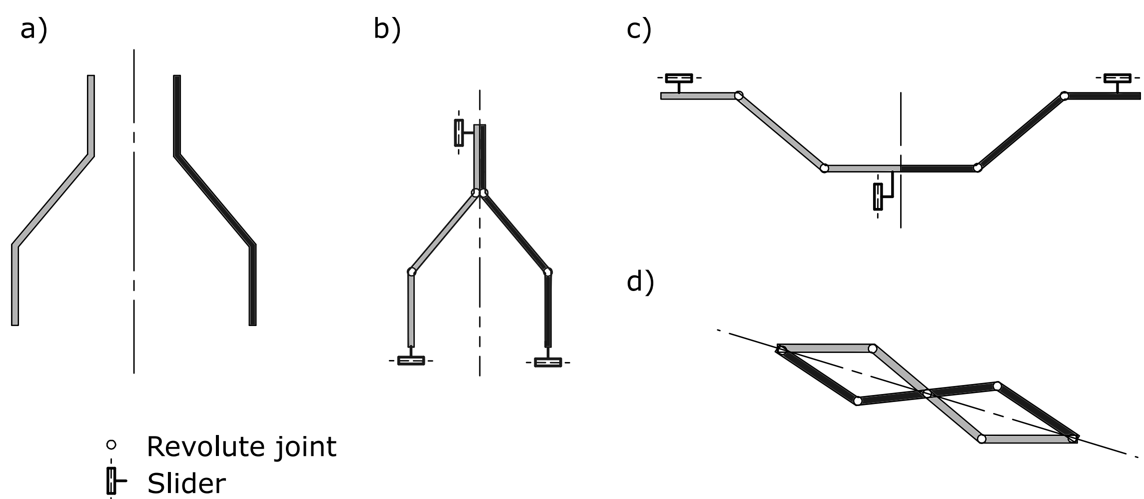

Fig. 5. Representation of (a) the two enantiomorphs, and the achiral meiotic bases (b) Lucky bone (Lb), (c) Rose (Ro), and (d) The Wine rack (Wr).

A_{1n} to the points $A_{2(n+1)}$. The case $2CRo$, where the classical Ro base structure is copy-rotated two times is represented in Fig. 7.c and is similar to $2CLb$ Fig. 6.c, however, $3CRo$ Fig. 7.d and $4CRo$ Fig. 7.e, etc. are different form the lucky bone designs, as are their tiling. For reasons similar to the Lb designs, the beams A_1A_1' and A_2A_2' are removed.

The Ro and Lb structures are equivalent, and if tessellated, one can find that the two designs are complementary to the other. However, in the higher order they can generate different types of structure. The edges are also different in the two structures, the Lb has edges as points whereas the Ro structures possesses planes. The differences in contact topology can help connections to other structures and enable the design of complex and user defined metamaterials. Moreover, the reciprocal Rose structures, with $N \geq 3$ possess, as the RLb, an anepirretic property, when tessellated, $4RRo$ correspond to $4RLb$ and, $3RRo$ correspond to $6RLb$.

3.1.4. Achiral "wine rack" (Wr) design

The meiotic "Wine rack" structures (Grima et al., 2008, 2011; Fortes et al., 2011; Lim, 2020), coded Wr, are built from the third achiralisation of Z_M (Fig. 5.a). The center of rotation O_R is located at the point A' or B' (Fig. 8.a), and the angle φ is the angle $\widehat{A_1A'A_2}$, and $\widehat{B_1B'B_2}$ for regular structures, the two angles can be different to create irregular Wr structures. The Wr structure is centrosymmetric at the point O, therefore the classical and reciprocal designs are identical for regular structures. Therefore, a convention can be taken, the classical structure as the center of rotation $O_R = A'$ and the edge point $E = B'$, whereas the reciprocal design has the center of rotation $O_R = B'$ and the edge point $E = A'$. For the regular designs, the names CWr and RWr can be simplified as Wr only. The case $2Wr$ (Fig. 8.a, b) was the one named wine rack design initially and corresponds to a scissors mechanism or pantograph structure (dell'Isola et al., 2015; Turco et al., 2016; Turco and Rizzi, 2016; dell'Isola et al., 2019). The representation of the topology of $3Wr$ is represented in Fig. 8.c and $4Wr$ in Fig. 8.d. The unit cell of $2Wr$ (Fig. 8.b) is constructed with the lines passing by $E_1 = B'$ and $E_2 = A'$ and the lines passing by (A_1A_2) and (B_1B_2), the unit cell design are constructed as detailed in Section 2 and illustrated for $4Wr$ in Fig. 8.d. An irregular variation of the wine rack structure was proposed (Dudek et al., 2016) with a Z_A possessing two different

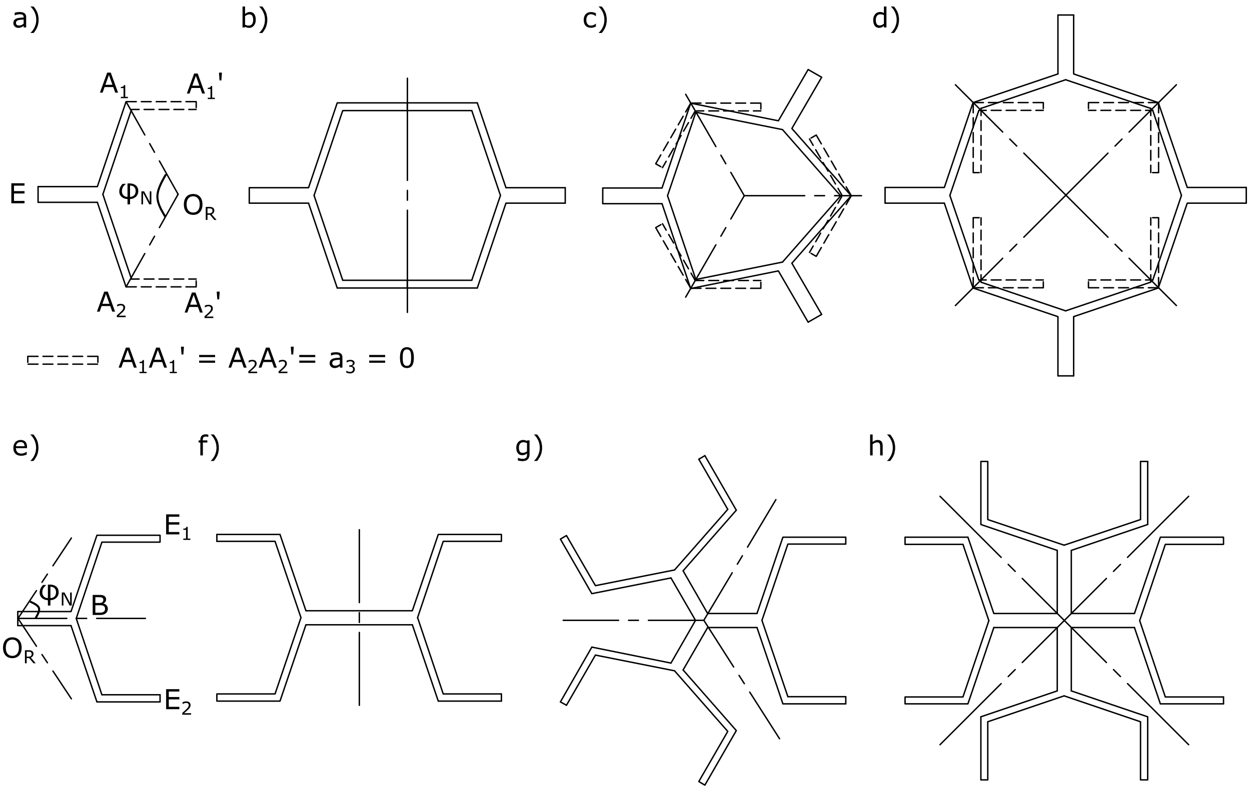

Fig. 6. Topological design of the regular achiral “Lucky bone” meiotic metamaterial, with (a) the creation of the center of rotation O_R with the points of interest. The representation of the copy-rotated structures for (b) $2CLb$, (c) $3CLb$ and, (d) $4CLb$ with the representation of the sacrificial beams. The construction of the reciprocal Lucky bones with (e) the position of the center of rotation O_R and the points of interest. The representation of the copy-rotated structures for the meiotic structure (f) $2RLb$, and the anepirretic structures (g) $3RLb$ and, (h) $4RLb$.

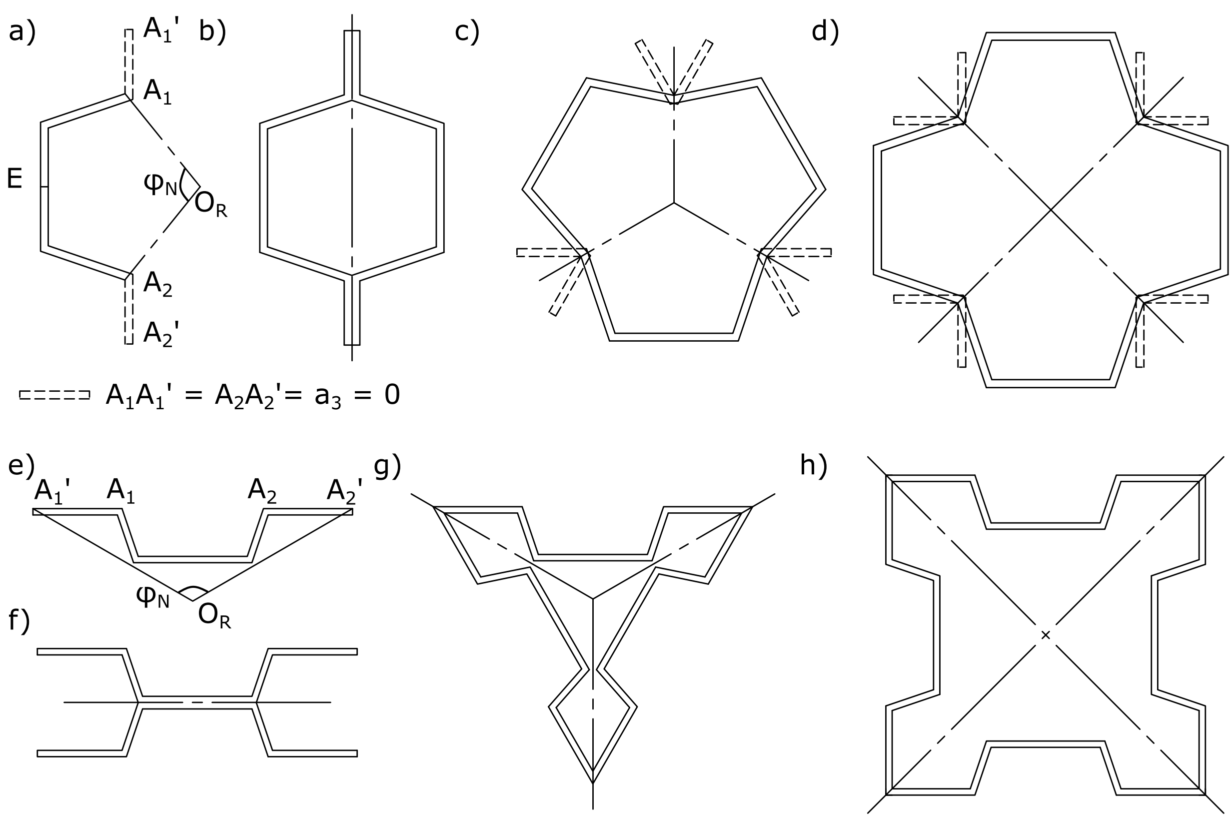

Fig. 7. Topological design of the regular achiral “Rose” meiotic metamaterial, with (a) the construction of the center of rotation O_R of the classical Rose (CRo) design and the points of interests. The representation the copy-rotated structures (b) $2CRo$, (c) $3CRo$, and (d) $4CRo$. The topological design of the reciprocal Rose (RRo) design with (e) the construction of the point of rotation, with the points of interests. The representation of copy-rotated structures (f) $2RRo$, (g) $3RRo$, and (e) $4RRo$.

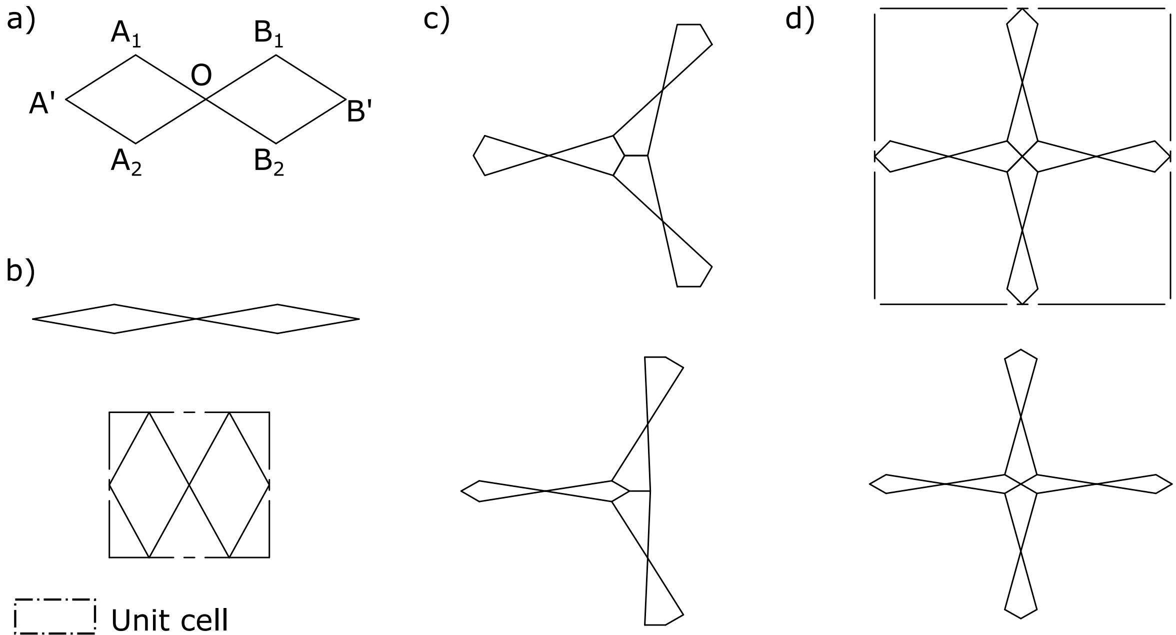

Fig. 8. Topological design of the regular achiral "Wine rack" meiotic metamaterial, with (a) the construction of the center of rotation O_R and the points of interests, and (b) the representation of Wr (equivalent to $2Wr$) at different deformation states with the unit cell structure. The representation of the copy rotated structures, in the undeformed state (top) and deformed state (bottom) of (c) $3Wr$, and (d) $4Wr$ with the design of the unit cell.

angles $\theta_1 \neq \theta_2$. The structure exhibits a high positive Poisson's ratio and a negative linear compressibility.

The Wr structure is composed of two rhombi, a variation could be to have only one rhombus which can be created from having Z_M with $a_1 = 0$ and $[OB_1] = a_2$. This irregular Wr structure could be called Snowflake (Sf), could be described as only one rhombus of the Wine rack design. Sf can be copy-rotated as an achiral structure four times to give the structure $4CSf$ which possesses an anepirretic behavior similarly to $4RCs$, because of the decoupling point at the center of the structure. $4CSf$ can be copy-rotated to the higher-order, for instance, into $4.4CSf$ (Giraud et al., 2022) which exhibit this time a meiotic behavior. The anepirretic or meiotic behavior is mainly dependent on the direction of the compression or stretch on the unit cell. The structure Sf is presented in Appendix C.

An other irregular structure can be designed from a variation of the position of the axis of symmetry while having the length a_3 (or a_1) set to zero. The initial axis is passing through the points A' and B', we propose to shift the position of the axis up or down and parallel, but not necessarily, to the initial one. Following the transformations one obtains the well known Scissor mechanisms, coded "Sm". We detail the position of the axis of symmetry and the topology in Appendix D.

3.2. Building chiral structures

Here, we present three main chiral families of design that originate from the chiral base Z_M, we illustrate how to create the center of rotations O_R and how to apply the copy-rotation protocol. The auxetic PPRDM produced three regular chiral auxetic structures the Missing-rib (Mr), the Closed-geometry (Cg), and the Honeycomb (Hc) (Roberjot and Herder, 2024). To be consistent with the auxetic PPRDM, we propose to follow the modifications applied to Z_A for its chiral transformation. We show that, even though these chiral structures are created from the meiotic base, they do not display a meiotic behavior but are auxetic.

3.2.1. Chiral "Missing-rib meiotic" (Mrm) design

The first chiral design uses the point A' (orB') as its center of rotation O_R, depending if the designer wishes to obtain a chiral or anti-chiral structure. The length a_3 of the beam BB' is set to zero to comply with the design method remove additional internal degrees of freedom. The angle φ_N is the angle of copy-rotation between two copy-rotated Z_M structures, i.e. $\varphi_N = \widehat{A_n O_R A_{n+1}}$, with A_n and A_{n+1} the point A of two adjacent copy-rotated Z_M structures, and $n \in [1, N]$ (Fig. 9.a). However, when copy-rotated following this scenario, the structures created have the similar topology as the Missing-rib (Mr) auxetic structures (Zhu et al., 2022; Wang et al., 2022), and possess, thus, an auxetic behavior. When it comes to naming this family, which is auxetic in the lower-order copy-rotation, one could use the Mr naming convention. However, we show that the higher-order achiralisation (Section 3.3.2) of these structures when Z_M has its angle $180 > \theta > \theta_{max}$, the copy-rotated structures possess a meiotic behavior. Therefore one could name the structures built with Z_M with an angle $180 > \theta > \theta_{max}$ as "Missing-rib meiotic" structures, coded "Mrm". The copy-rotation process is illustrated for $Mrm3$ in Fig. 9.b, and $Mrm4$ in Fig. 9.c.

The base structures Z_A and Z_M can be also copy-rotated with their one edge A' (orB'), in that case without putting the length of the opposite beam to zero, can be named for instance for four copy-rotations Z_A4 or for six copy-rotations Z_M6.

3.2.2. Chiral "Closed-geometry meiotic" (Cgm) design

The second chiral design uses the center of rotation O_R at the tip of the isosceles triangle $A'O_RB'$ with the angle $\varphi_N = \widehat{A'O_RB'}$, illustrated in Fig. 10.a. The beams $B_nB'_n$ are rigidly connected to the beams $A_{n+1}A'_{n+1}$. Similarly to the Mrm family, when Z_M is copy-rotated following this process, the structures that are created possess the same topology as the auxetic Closed-geometry (Cg) family. The higher-order achiralisation (Section 3.3.2) of these structures also leads to a meiotic behavior, and therefore, the structures could be named, for structures created with Z_M with their angle $180 > \theta > \theta_{max}$, as "Closed-geometry meiotic" coded "Cgm". The copy-rotation process is illustrated for $Cgm3$ in Fig. 10.b, and for $Cgm3$ in Fig. 10.c.

The regular unit cells of the Cgm and Cg families are defined as passing by the edge points E_N and being colinear to the beam where E_N is on. However, using such a regular unit cell for the tessellation is limiting the range of dimensions of a_1, a_2 and a_3, indeed, for certain

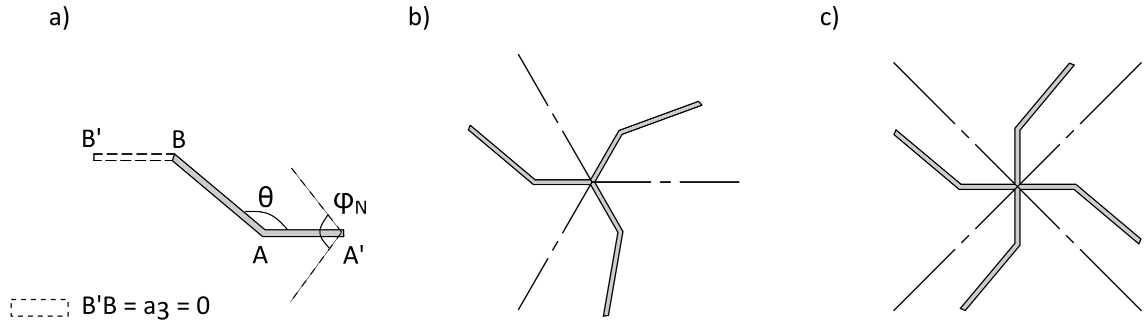

Fig. 9. Topological design of the regular chiral "Missing-rib meiotic" metamaterial, with (a) the construction of the center of rotation O_R and the copy-rotation of the cases (b) $Mrm3$ where $N = 3$ and, (c) $Mrm4$ where $N = 4$.

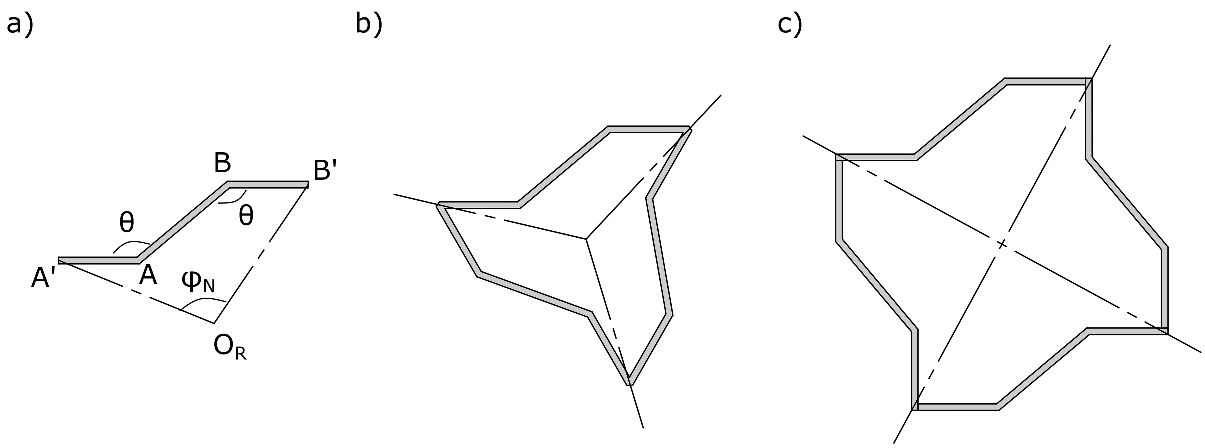

Fig. 10. Topological design of the regular chiral "Closed-geometry meiotic" metamaterial, with (a) the construction of the center of rotation O_R and the copy-rotation of the cases (b) $Cgm3$ where $N = 3$ and, (c) $Cgm4$ where $N = 4$.

cases the structures can be non connecting because of internal connections. Irregularities can be brought to the tessellations that brings a more natural tiling scheme. The edges E_N are located at the middle of the beams BB', the irregular tessellation connects the points E_N rigidly and the beams become colinear and rigidly linked. The regular and irregular tessellations are presented in Appendix E.

3.2.3. Chiral "Honeycomb meiotic" (Hcm) design

The third chiral design uses the center of rotation O_R at the tip of the isosceles triangle AO_RB with the angle $\varphi_N = \widehat{AO_RB}$, illustrated in Fig. 11.a. The length a_3 of the beam BB' is set to zero to comply with the design method and prevent adding additional internal degrees of freedom. To create anti-chiral structures, the length a_1 is set to zero, instead of a_3. However, when copy-rotated following these rules, the structures created has a similar topology of the auxetic Honeycomb (Hc) structures (Roberjot and Herder, 2024). And, as for the Mrm and Cgm family, the higher-order achiralisation process enables the meiotic behavior to happen. Therefore, we adapted, here too, the naming convention. The structures created with Z_M with an angle $180 > \theta > \theta_{max}$, could be named "Honeycomb meiotic" coded "Hcm". The copy-rotation process is illustrated for $Hcm3$ in Fig. 11.b, and $Hcm4$ in Fig. 11.b. The center body is considered as one single rigid body as for the Hc design, however, it could be set a flexible body which could possibly lead to reducing the auxetic behavior and even to express meioticity.

An irregular structure (Hcm_I) can be formed here if the beam BB' (orAA') is kept to a non null length. The difference between the Hc auxetic family is that the beam which is set to zero length is not inside the center rigid body and therefore could be used to form more complex structures. The irregular Hcm_I design is detailed in Appendix F. Hcm_IN possesses two "legs" per sector and the shape of its unit cell has the same topology as the "Closed geometry" chiral auxetic structure CgN. Hcm_I is used in the design of origami structures, indeed it represents the crease line pattern of some rotating origami (Silverberg et al., 2015; Zhang et al., 2020). In the case of a non-rigid internal body, the metamaterials correspond to the 2D projection of the base structures used for reconfigurable prismatic metamaterials (Overvelde et al., 2016, 2017; Zhu et al., 2019).

In addition, the achiralisation of these irregular Hcm_I structure can lead to the design of a novel achiral meiotic structure, which resembles to Butterfly wings. The Butterfly design (Bt) is depicted in the Appendix G.

3.3. Higher-order Poisson's ratio metamaterials

Higher-order Poisson's ratio metamaterials can be designed following the third step of the design method, detailed in Section 2.2, using the copy-rotation and achiralisation geometrical transformations. We present, first, the higher-order copy-rotation process with some examples or achiral and chiral structures, second, the achiralisation process for some structures and discuss about their Poisson's ratio behavior, and finally, we discuss the design of hierarchical and fractal metamaterials.

3.3.1. Higher-order copy-rotation

The higher-order copy-rotation can be applied to the chiral and achiral structures to create specific metamaterials. The point of rotation O_R is defined in a similar manner as for the low-order Poisson's ratio structures. For achiral metamaterials, and if the base structure is follows a classical design, with one edge E per face of the unit cell, O_R is located at the edge point E. In the case of a reciprocal base design, the center of rotation is chosen as a classical O_R, meaning that O_R is built from two edges forming an angle $\varphi_N = \widehat{E_1O_RE_2}$. In the

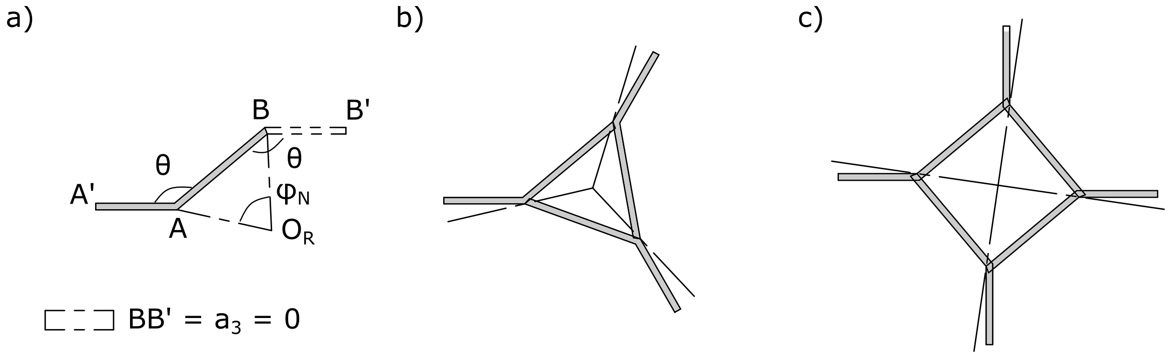

Fig. 11. Topological design of the regular chiral "Honeycomb meiotic" metamaterial, with (a) the construction of the center of rotation O_R and the copy-rotation of the cases (b) $Hcm3$ where $N = 3$ and, (c) $Hcm4$ where $N = 4$.

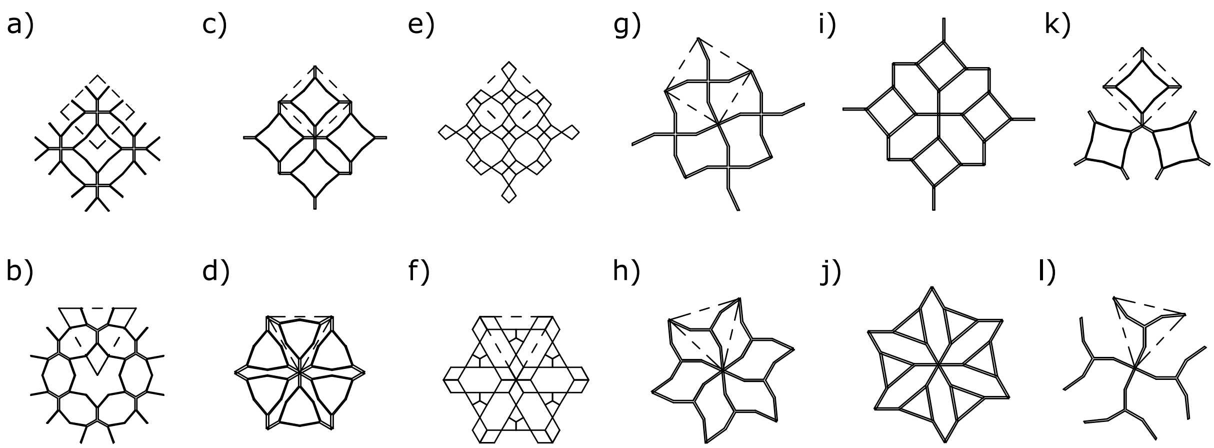

Fig. 12. Representation of the topology of the regular achiral higher-order (a) $4.4RLb$, (b) $6.3RLb$, (c) $4.4CLb$, (d) $6.3CLb$, (e) $4.4Wr$, and (f) $6.3Wr$. Representation of the regular chiral higher-order (g) $Mrm4.4$, (h) $Mrm3.6$, (i) $Hcm4.4$, and (j) $Hcm3.6$. The example of two irregular topologies (k) $3.4CLb$, and (l) $Mrm3.4$.

two cases the position of O_R follows the rules of the metastructure's family. The number of higher-order copy-rotation is dependent on the order of the base structure, an N order regular structure possess a N order regular unit cell which defines the angle φ_N between two faces of the UC. That angle is conserved in the higher-order copy-rotation, therefore, the copy-rotation is limited to a maximum of M repetitions of φ_N, with $M\varphi_N \leq 360°$ (See Section 2.2). Because of that condition the structure $6.3CLb$ exists, the angle φ_3 of $3CLb$ is 60°, the higher-order copy-rotation exists for $M \in [6, 2[$, the cases $M = 2$ correspond to a tessellation of the structure, and the case $M = 1$ is not affecting the structure. Examples of some higher-order copy-rotation of classical and reciprocal structures are illustrated, for $4.4RLb$, $6.3CLb$ and the irregular $3.4CLb$ and $5.3RLb$, in Fig. 12.a–f.

For the chiral structures, the principle is the same, the point O_R is located at the edge point E. The higher-order copy-rotated chiral structures are also presenting an auxetic behavior, as the structures possess the same chirality and, the higher-order copy-rotation enables a variation of the tessellation compared to the tessellation of the "low" order structures. For instance, the case $Cgm4.4$ has the same tessellation as $Cgm4$, only the thickness of the beams is theoretically changing because of the process. Examples of higher-order chiral structures are illustrated, for Mrm and Hcm in Fig. 12.g–j.

Irregular higher-order structures can be designed using a mismatch between the copy-rotation, for example the Fig. 12.k shows the structure $3.4CLb$, creating a triangular unit cell from a square base, adaptations needs to be done to tessellate the structure or to connect it to another type of structure to act as a joint, the Fig. 12.l shows a chiral irregular higher-order structure $Mrm3.4$.

3.3.2. Higher-order achiralisation

In addition to the higher-order copy-rotation, the chiral structures (Section 3.2) can be achiralised to form a higher-order achiral base, which can then be copy-rotated. The process of achiralisation is similar to the one used for the creation of the achiral bases (Section 3.1.1), it requires the creation of a line passing through at least one point of the chiral structure, to mirror the structure, thus combining the two enantiomorphs This process was explored for auxetic structures (Broeren et al., 2020). The achiralisation process can be applied to the three chiral families Cgm, Hcm and, Mrm and their higher-order copy-rotated transformations.

The chiral Cgm structures can be achiralised following the same process as for the auxetic Cg family, the mirror line is passing through the points B_n and B'_n (or A_n and A'_n for anti-chiral structures) (Section 3.2.2). The achiralisation process applied to the Cgm family gives the structures presented in Fig. 13.a.b detailing the position of the points O_{RC} and O_{RR} with the topology of some copy-rotated structures Fig. 13.c–f. The meiotic behavior of the structure $2CACgm4$ (Fig. 13.e) is presented in Fig. 15 and detailed in Appendix H. The meiotic behavior is found in these structures because of the presence of the $2CLb$ structure created by the achiralisation.

However, we have shown that the chiral structures created with our design method from the structure Z_M possess an auxetic behavior (Section 3.2), and the risk would be that achiralising these auxetic chiral structures leads to structures that are also auxetic, limiting thus the possibility for designing meiotic structures.

The chiral auxetic structures that were achiralised share two design aspects, first the angle between the mirror line and one of the leg is of 90°; second, the joined beams are rigidly linked during the achiralisation process. Following these rules leads to have one rigid

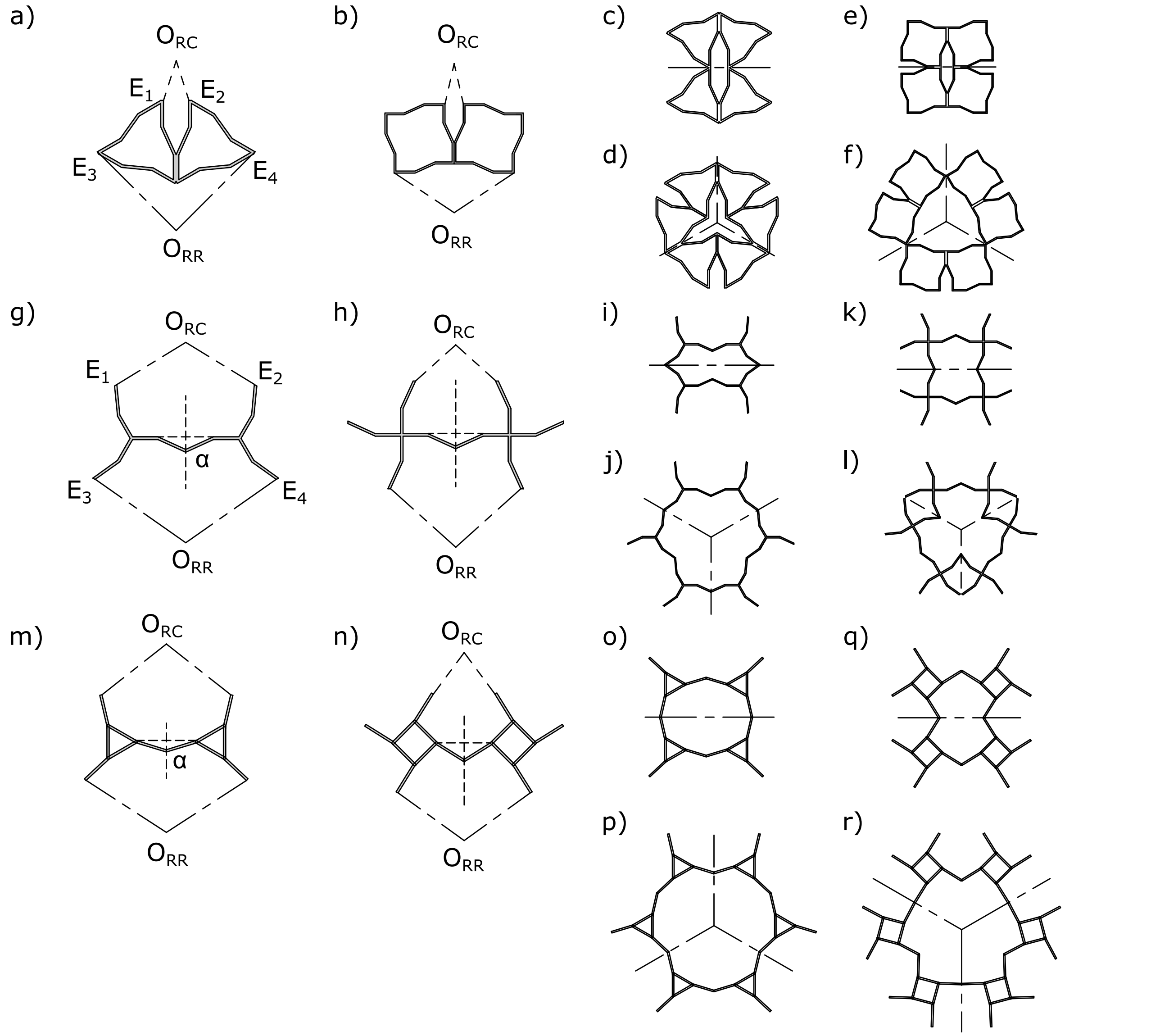

Fig. 13. Representation of the achiralisation process of the Cgm family with the representation of the points O_{RC} and O_{RR} for the structures (a) $ACgm3$, and (b) $ACgm4$, and the representation of the higher-order copy-rotated structures (c) $2CACgm3$, (d)$3RACgm3$ (which is equivalent to $3CACgm3$), (e) $2CACgm4$, and (f) $3RACgm4$. Representation of the achiralisation process, with the axis of achiralisation non normal with the beam of the Mrm family with the representation of the points O_{RC} and O_{RR} for the structures (g) $AMrm3$, and (h) $AMrm4$, and the representation of the higher-order copy-rotated structures (i) $2RAMrm3$, (j) $3RAMrm3$, (k) $2CAMrm4$, and (l) $3CAMrm4$. Representation of the achiralisation process of the Hcm family, with the axis of achiralisation non normal with the beam, with the representation of the points O_{RC} and O_{RR} for the structures (m) $AHcm3$, and (n) $AHcm4$, and the representation of the higher-order copy-rotated structures (o) $2CAHcm3$, (p) $3CAHcm3$, (q) $2CAHcm4$, and (r) $3RAHcm4$.

beam that usually does not deform when compressed or stretched and confers the achiralised structures with an auxetic behavior.

Therefore, we introduced some irregularities while using the achiralisation process, detailed in Section 2.2. If the achiralisation axis is normal to the beam where the edge point is, the achiralised structures are connected rigidly. However, if the axis of achiralisation is not normal to the beam, then the achiralised structures are linked with a revolute joint.

The chiral structure are mirrored with an axis passing through the edge of one leg of the Mrm or Hcm structures and be normal to the line $O_R A$ (Fig. 13.g.h.m.n), creating an angle $\alpha \neq 90°$ between the mirror line and the leg.

The achiralised structures that are created following a non normal achiralisation have their beams $O_R A$ colinear, and when stretched or compressed along that line, theoretically, does not have internal rotation. Preventing the internal twist leads to having only the deformation coming from the offset of the angle $\alpha = \widehat{A_1 A' A_2}$ between the two legs, with A'_1 and A'_2 belonging to the two enantiomorphs.

Illustrations of the copy-rotations of some achiralised structures are presented in Fig. 13.i–l for the Mrm family, and in Fig. 13.o–r for the Hcm family.

The position of the mirror line enables to gain meioticity from the chiral auxetic structures, however, for square structures an other behavior is gained, they present an anisotropic Poisson's ratio behavior where the value of PR is positive in one direction and negative in the other. This effect is detailed in Section 3.4.2. The meiotic behavior of the structure $2CAMrm4$ (Section 3.3.2.k) is presented in Fig. 15 and detailed in Appendix H.

3.3.3. Hierarchical and fractal meiotic metamaterial structures

Hierarchical structures are formed by assembling structural elements, which themselves possess a nested structure (Gatt et al., 2015a; Li et al., 2021). Hierarchical meiotic structures, akin to hierarchical auxetic structures (Hamzehei et al., 2018), are obtained from chiral structures through a series of transformations. These transformations include a minimum of two levels of copy-rotation, followed by an

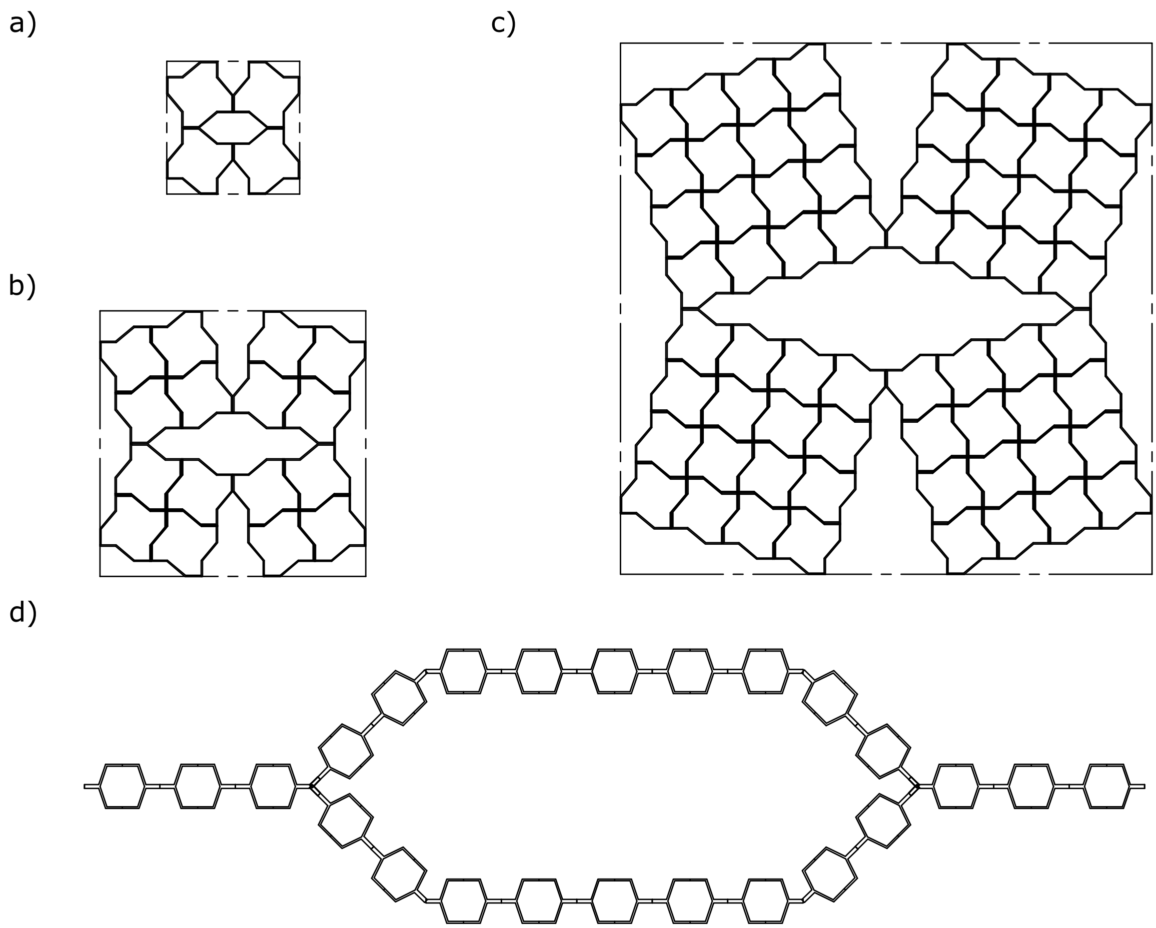

Fig. 14. Geometrical representation of the hierarchical structures, with their unit cells, (a) $2CACgm4$, (b) $2CACgm4.4$ (c) $2CACgm4.4.4$, and (d) an example of the representation of the two levels fractal structure of $2CLb$.

achiralisation process, and concluding with an additional copy-rotation step.

For instance, $Cgm4$ can form hierarchical structures, $Cgm4$ can first be achiralised and copy-rotated two times to form $2CACgm4$ (Fig. 14.b), but $Cgm4$ can be copy-rotated four times in its chiral topology to form $Cgm4.4$, to be achiralised and copy-rotated two times again (Fig. 14.b). The process can be applied further, one may copy-rotate $Cgm4.4$ four times to create $Cgm4.4.4$ then achiralising it, and copy-rotating the structure two times to design $2CACgm4.4.4$ (Fig. 14.c) Contrary to auxetic structures, which structures can be chiral or achiral, the planar meiotic metamaterials are limited in, except for Z_M, achiral structures. The hierarchical structures proposed here, have a meiotic design, however, they possess chiral, thus auxetic, sub-components. The design of such mixed structures can be interesting to first control the Poisson's ratio behavior, and also, the deformation and overall mechanical behavior of the metamaterial. In Appendix I another type of hierarchical metamaterial is presented form the structure $4.4.2CACgm4$ with particular hinge points (Jalali et al., 2022), the structure possess an overall auxetic mechanism with internal achiral meiotic structures.

Fractal structures are self-replicating patterns found at all scales, and are abundant in both natural and engineering contexts (Mandelbrot, 1983; Wang et al., 2022). These proposed meiotic designs can serve as fundamental building blocks for creating larger-scale structures with the same design. The Fig. 14.c represents a two layers fractal structure of $2CLb$, meaning that if a zoom image of $2CLb$ is taken, the structure $2CLb$ will be found at a smaller scale. Fractal metamaterials allows the combination of motion over a deformation, which could be perceived as a product of motion, whereas the hierarchical structures employ a summation of motion. Both hierarchical and fractal auxetic metamaterials offer intriguing possibilities for controlling and programming the deformation behavior of PR metamaterial structures.

3.4. Poisson's ratio, surface strain and negative compressibility

In this section, we explore first, through five examples of meiotic structures (Z_2, $2CLb$, $4CLb$, $4RLb$, $4CACgm4$ and $4CAMrm4$), the calculation of the Poisson's ratio ν, surface strain ε_S, and finally discuss the sign of their compressibility. Second, we detail and discuss the anisotropic Poisson's ratio behavior that the chiral meiotic structures gain through the process of achiralisation.

3.4.1. Calculation of Poisson's ratio, surface strain and compressibility

We are calculating here the Poisson's ratio ν and surface strain ε_S for seven structures. The structures possess an initial angle $\theta_I = 90°$ and length $a_1 = a_2 = a_3 = 1$. The initial angle is selected at 90° therefore the value ε_θ defined as

$$\varepsilon_\theta = \frac{\theta - \theta_I}{\theta_I} \tag{11}$$

is negative ([−1,0]) for the auxetic region and positive ([0,1]) for the meiotic region. We propose to give the derivation for Poisson's ratio and surface strain for a few structures. First, the derivation for the base structure Z_2 was given in Section 2.1. The example of the derivation is given here for the structure $2CLb$, the derivations for the other structures are detailed in Appendix H. The structure exists in the auxetic region as $2CCs$. The length and height of the structure $2CLb$ (Fig. 15.a.b.c) can be written as a function of the angle θ as

$$L(\theta) = 2\left(a_1 + a_3 - a_2\cos(\theta)\right) \tag{12}$$

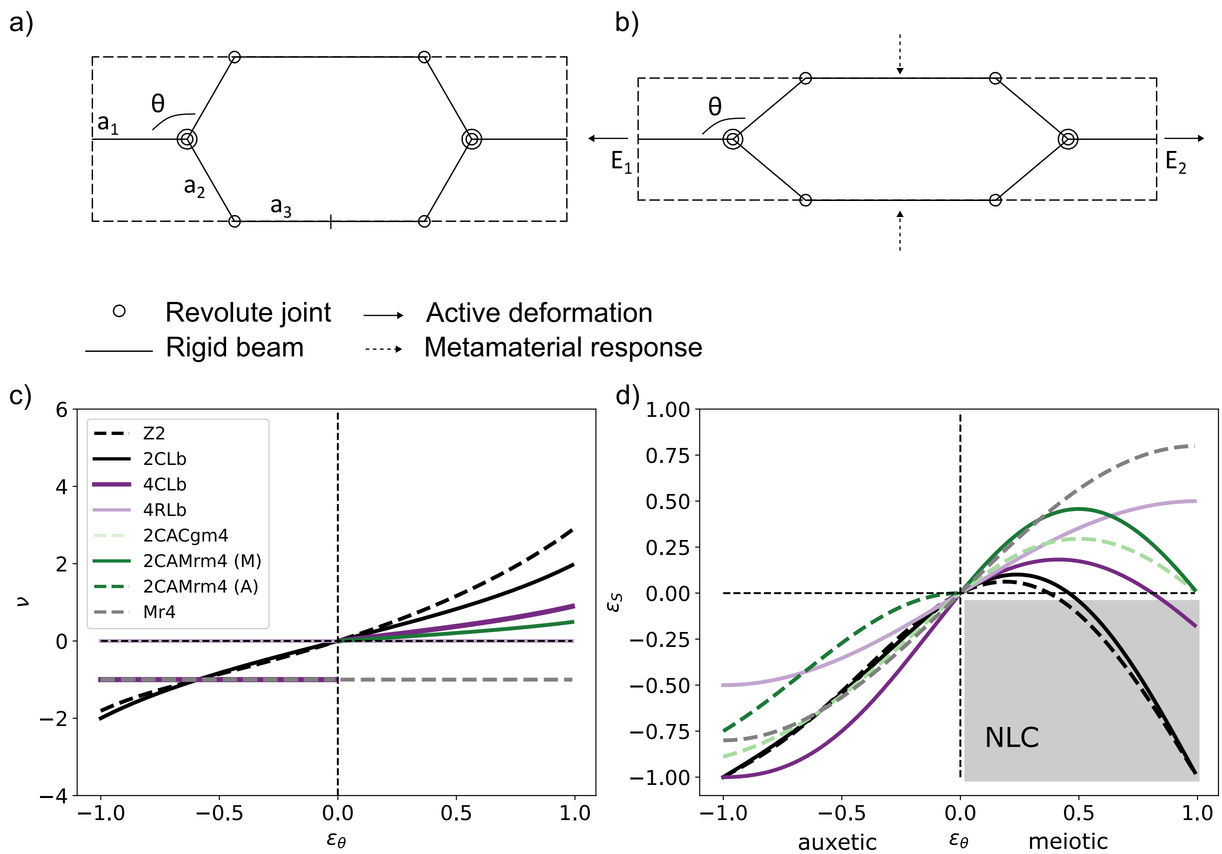

Fig. 15. Kinematic representation of the structure $2CLb$, with its parameters, (a) undeformed, and (b) deformed. Evolution of (c) the Poisson's ratio (ν) and (d) the surface strain (ε_S) of the meiotic structures Z_2, $2CLb$, $4CLb$, the auxetic structure $Mr4$, the anepirretic structure $4RLb$, and the anisotropic structures $2CACgm4$, $2CAMrm4(M)$ and $2CAMrm4(A)$.

$$H(\theta) = 2a_2 \sin(\theta) \tag{13}$$

The value of the strains are

$$\varepsilon_L(\theta) = \frac{L(\theta)}{L(\theta_I)} - 1 \tag{14}$$

and

$$\varepsilon_H(\theta) = \frac{H(\theta)}{H(\theta_I)} - 1 \tag{15}$$

The Poisson's ratio $\nu(\theta)$ can thus be written as

$$\nu(\theta) = -\frac{\varepsilon_H(\theta)}{\varepsilon_L(\theta)} \tag{16}$$

The equations of length and height enable to calculate the surface strain $\varepsilon_S(\theta)$ of the rectangular unit cells of $2CLb$ and $2CCS$ as

$$\varepsilon_S(\theta) = \frac{L(\theta)H(\theta)}{L(\theta_I)H(\theta_I)} - 1 \tag{17}$$

The value of the Poisson's ratio for different values of θ are presented in Fig. 15.c and the evolution of the surface strain in Fig. 15.d for the seven structures.

The surface strain gives information that link to the surface compressibility of the metamaterial. The isothermal surface compressibility β_S is defined as

$$\beta_S = -\frac{1}{S}\left(\frac{\partial S}{\partial P}\right)_T \tag{18}$$

assuming the temperature constant, it can be written as

$$\beta_S = -\frac{\varepsilon_S}{\sigma_S} \tag{19}$$

with ε_S the surface strain and σ_S the stress or load applied to the structure. The surface bulk modulus K_S is defined as the inverse of the surface compressibility

$$\beta_S = \frac{1}{K_S} \tag{20}$$

When the structure is stretched, the stress applied is negative, therefore, if the surface strain is negative too, the compressibility becomes negative (oppositely for a compression). The metamaterials exhibit in this case a negative linear compressibility (NLC) (Baughman et al., 1998; Lakes and Wojciechowski, 2008).

First, we note that the base structure Z_2 is indeed auxetic when $\theta_T < 90°$ (corresponding to the transition angle for $a_1 = a_2 = a_3$), and is meiotic when $\theta_T > 90°$, and possess a Poisson's ratio greater than the other structures studied here. The base chiral structures possess a positive compressibility in the auxetic region and showcase a NLC behavior when meiotic. In addition we observe that the Poisson's ratio of $2CCs/2CLb$ is negative for $\varepsilon_\theta < 0$ and positive for $\varepsilon_\theta > 0$. In addition, the surface strain is negative for $\varepsilon_\theta < 0$ indeed the structure $2CCs$ shrinks in all directions when hydrostatically compressed, however, when $\varepsilon_\theta > 0$, $2CLb$ possess initially a positive surface strain (positive compressibility) and around $\varepsilon_\theta = 0.5$ becomes negative, this is when the structure obtain negative linear compressibility. the values of the initial angle and length of the beams could be adapted to design structures that are engaged in the NLC region earlier or later. In addition, the region where $\varepsilon_\theta < 0$ and $\varepsilon_S > 0$ is not reachable with mono-material structures, this would lead to a negative compressibility when auxetic, leading to a negative Young's modulus. However, it has been shown that a bi-material structure could reach this region (Gatt and Grima, 2008).

We present the evolution of Poisson's ratio and surface strain for the structures $4CLb$, $4RLb$, $2CACgm4$ (presented in Appendix H), $Mr4$ which is a chiral structure and always auxetic and the anisotropic structures $2CAMrm4$ presented in Section 3.4.2.

Surface strain provides additional insights into the behavior of metamaterials. The Poisson's ratio offers geometric information regarding deformation and, structures may present a similar Poisson's ratio behavior, such as $4CLb$ and $2CACgm4$. However, their surface strain behaviors differ. A comprehensive understanding of surface strain opens up the opportunity to tailor the design of metamaterials, especially for large tessellations of small unit cells.

3.4.2. Anisotropic Poisson's ratio metamaterials (ani-PRM)

We have been showing in Section 3.2 that the chiral structures originating from Z_M become auxetic instead of being meiotic. This aspect of chiral metamaterials leads to the hypothesis that, except for Z_M, the meiotic structures cannot be chiral. The achiralisation of the chiral structures Cgm, Hcm and Mrm following the rules given in Section 3.3.2 is leading to a meiotic behavior and a noteworthy anisotropic Poisson's ratio behavior for Hcm and Mrm. The structures $2CAMrm4$ and $2CAHcm4$ (as probably some more structures of these family) are presenting an anisotropic Poisson's ratio behavior. The structure $2CACgm4$ does not seem to exhibit this behavior because of the absence of edge points located on free legs Appendix H.

The Poisson's ratio of such metamaterials could be described in two ways. The first, where the two Poisson's ratio ν_A (for auxetic) and ν_M (for meiotic) are linearly related as $\nu_{xy} \approx -a_\nu \nu_{yx}$, where the Poisson's ratio have an opposite sign and a_ν the anisotropy coefficient. Second, where the two Poisson's ratio are not linked by a coefficient but are two different Poisson's functions. These metamaterials can be subcategorized as anisotropic Poisson's ratio metamaterials (ani-PRM), and defined as metamaterials with a direction dependent Poisson's ratio.

These structures possess a square unit cell and present in two opposite faces (F_1 and F_3) edge points that are closer than the edge points on the two other opposite faces (F_2 and F_4). The edge points that are closer are located on the faces named F_M (for meiotic), oppositely, the edge points that are further away are located on the faces F_A (for auxetic).

The structure $2CAMrm4$ is detailed here, however the similar principles apply to the structures $2CAHcm4$ and the structure $2CACgm4$ (Appendix H) for its meiotic behavior. The structure $2CAMrm4$ (Fig. 16.b) possesses eight edges, $E_1 - E_4$ are located on the two faces F_M, and $E_5 - E_8$ are located on the two faces F_A. The achiralisation and copy-rotation of the $Mrm4$ structures creates four internal triangular shapes (forming the angle α_M and α_A), that are pointing towards the center if located in the sector of a face F_M and are pointing towards the face of the unit cell if located in the sector of a face F_A. The angle $\alpha = 0°$ when $\theta = 90°$.

When stretched (or compressed) in the direction normal to the faces F_M the structures (Fig. 16.a) $2CAMrm4$ deploys (or contracts) and the internal structure tends to align on the line (E_1E_3) and (E_2E_4), while keeping the same distance between these two lines. The initial length and height are equal because of the symmetry (for regular structures)

$$L(\theta_I) = H(\theta_I) = 4\left(a_3 + a_2\cos(\theta_I)\right) \tag{21}$$

Upon stretching (or compressing) the angles α_M are closing (or opening), while the angles α_A are opening (or closing). The opposite behavior of α_M and α_A is leading to elongating (narrowing) the structure in the direction of the stretch (or compression) and narrowing (or expanding) the transverse direction. The final length becomes then

$$L(\theta) = 4\left(a_3 + a_2\cos(\theta)\right) \tag{22}$$

and the height

$$H(\theta) = 4\left(a_3 - a_2\cos(\theta)\right) \tag{23}$$

The strain ε_L can be written as

$$\varepsilon_L(\theta) = \frac{L(\theta)}{L(\theta)} - 1 = \frac{a_3 - a_2\cos(\theta)}{a_3 - a_2\cos(\theta)} - 1 \tag{24}$$

and the strain ε_H as

$$\varepsilon_H(\theta) = \frac{H(\theta)}{H(\theta)} - 1 = \frac{a_3 - a_2\cos(\theta)}{a_3 - a_2\cos(\theta)} - 1 \tag{25}$$

Thus the meiotic Poisson's ratio ν_M is

$$\nu_M = -\frac{\cos(\theta) - \cos(\theta_I)}{\cos(\theta) - \cos(\theta_I)} \tag{26}$$

ν_M is positive and depends on the value θ, the behavior of $2CAMrm4$ is then meiotic when the deformation is activated on the faces F_M.

However, when these achiralised structures are stretched (or compressed) along the faces F_A (Fig. 16.c), meaning stretching (or compressing) the structures on the lines (E_5E_7) and (E_6E_8) while keeping the same distance between these lines. With the initial length and height

$$L(\theta) = H(\theta) = 4\left(a_3 - a_2\cos(\theta)\right) \tag{27}$$

The angles α_A and α_M are all opening (or closing), thus the angles θ are opening to $\theta + \delta$. These similar behavior of the internal structure is leading to an auxetic behavior where the final length and height are theoretically equals and written as

$$L(\theta,\delta) = H(\theta,\delta) = 4\left(a_3 - a_2\cos(\theta)\right) \tag{28}$$

In that case, the structure $2CAMrm4$ exhibits an auxetic behavior.

The Poisson's ratio and surface strain of these two cases $2CAMrm4(A)$, and $2CAMrm4(M)$ are plotted in Fig. 15.c.d, the Poisson's ratio of this structure in the auxetic mode is theoretically constant to the value of $\nu_A = -1$, however the meiotic mode is close to 1 and decreases with δ.

4. Discussion

The proposed three-step design protocol is centered around two key topological transformations: achiralisation and copy-rotation. This approach opens up endless possibilities for creating meiotic planar metamaterials. However, many of these structures, particularly those with higher geometrical orders, cannot be tessellated with regular tiling. Meiotic structures with a high geometrical order possess a large number of internal degrees of freedom, this effect may lead to complex deformation schemes and may be more difficult to control or actuate. Nevertheless, we believe that these complex structures hold potential for specific applications, owing to their designed Poisson's ratio, deformation scheme, or compressibility.

Although our focus has primarily been on regular topological designs, the introduction of irregularities can lead to even more unique and specialized meiotic structures. These irregularities can be introduced geometrically by slightly modifying the axis of symmetry, or incorporating mismatches in lengths and angles, or through modifications to the copy-rotation protocol where each of the N repeated entities behaves uniquely in each of the N directions. Additionally, the higher order copy-rotation protocol with $N.M$ copy-rotations (when $N \neq M$) can also introduce irregularities, although it may necessitate adjustments to the structure to form a tessellable unit cell.

Naming conventions for irregular structures may require adaptation to reflect classes of irregularities. For example, the addition of a subscript I or including a specific detail in the name to identify a design variation.

We presented a design method for the unit cells of the planar Poisson's ratio metamaterials, along with the archimedean tiling, which enables regular and non-regular tiling in the plane of one or many different types of PRM. To connect different families of PRM structures together, the designs need to be adapted to have functional interfaces that connects to the adjacent unit cells. The possibilities for the design of planar PRM seem endless regarding, first, the possibilities offered by our design method and, second, by the possibilities of tiling these designs.

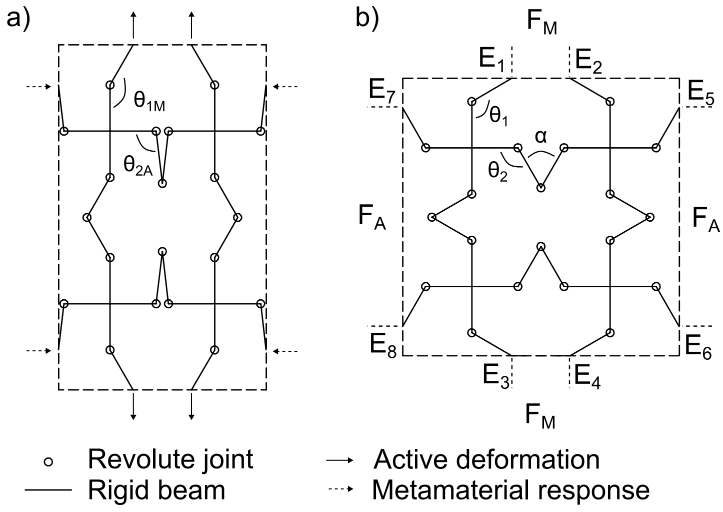

Fig. 16. Kinematic representation of the anisotropic Poisson's ratio metamaterial $2CAMrm4$ in (a) the meiotic deformation, (b) undeformed, and (c) in the auxetic deformation.

We have shown that, except for Z_M, the chiral planar structures produced by the design method do not possess a meiotic behavior, but are auxetic. The achiralisation process applied to the chiral families modifies the complexity of their unit cell and the resulting metamaterials gains an exceptional anisotropic Poisson's ratio behavior, which enables a change of sign of the Poisson's ratio depending on the direction of the stretch or compression.

Some structures, for instance, $4RLb$ (Section 3.1.2) and $4CSf$ (Appendix C) present an exceptional anepirretic behavior, these structures exhibit a Poisson's ratio of constant value of zero. The creation of such structures was enabled by the exploration of the possibilities offered by the PPRDM. We discussed this noteworthy behavior at the level of the structure itself, and shaping a unit cell. However, such a behavior needs to be investigated in a tessellation to understand how and where such a behavior can be used.

The meiotic structures we introduced present a Poisson's ratio higher than 0.5, a negative surface strain and therefore a negative compressibility behavior. Following perfectly the design method leads to creating regular and symmetric structures, however, some irregularities can be introduced to control the direction of the deformation and therefore the direction of elongation in negative compressibility applications. We have been showing that negative compressibility could happen when the structure present meioticity, when $\varepsilon_\theta > 0$ and $\varepsilon_S < 0$, however the region where $\varepsilon_\theta < 0$ and $\varepsilon_S > 0$ is not attainable, and would results in metamaterials possessing a negative Young's modulus. A metastructures exhibiting such property have been introduced (Gatt and Grima, 2008) with the use of multi-material metamaterial, a meta-composite.

2D structures with a constant or specific evolution of Poisson's ratio of could possibly be engineered using the design scheme proposed here. Controlling the deformation of odd N copy-rotation and large N meiotic structures will need to be addressed to gain understanding to use these structures in specific applications.

We considered the PPRDM for the creation of planar auxetic, anepirretic, and meiotic metamaterials based on a planar chiral structure. It would be interesting to consider an extension of the design method to 3D Poisson's ratio metamaterials. It is likely that a similar approach could be developed, to design, classify, name and tessellate such structures in 3D.

5. Conclusion

In summary, we present a systematic framework for the design and classification of meiotic structures, bridging their geometric properties with auxetic metamaterials. Through the use of a minimal chiral structure (Z_M) and a design method (PPRDM) based on two topological transformations, we generate a rich library of meiotic, anepirretic, and auxetic architectures.

Our approach enables not only the reconstruction of known meiotic forms but also the design of previously unexplored configurations, accommodating minor structural irregularities. We classify these structures according to chirality, showing that chiral configurations exhibit auxetic behavior, with the base structure uniquely combining chirality and meioticity. Achiral structures, in contrast, can display meiotic and anepirretic behavior.

To aid in systematic identification, we introduce a naming convention that encodes the structure's type, chirality, and topological complexity. Furthermore, we detail a construction protocol for unit cells and planar tessellations of 2D meiotic structures. Importantly, we propose the surface strain of the unit cell as a unifying metric for planar Poisson's ratio metamaterials, directly linked to the metamaterial's bulk modulus and compressibility. We propose the calculation of the Poisson's ratio and surface strain for a group of structures and show that some structures could exhibit indeed negative compressibility.

Together, these results establish a foundational design framework for planar meiotic metamaterials, opening new avenues for materials with programmable behavior, negative compressibility and other unconventional mechanical responses.

CRediT authorship contribution statement

Pierre Roberjot: Writing – review & editing, Writing – original draft, Visualization, Methodology, Investigation, Formal analysis, Conceptualization. **Just L. Herder:** Resources, Project administration, Methodology.

Declaration of competing interest

The authors declare that they have no known competing financial interests or personal relationships that could have appeared to influence the work reported in this paper.

Acknowledgments

This publication is part of the project Mechanical Metamaterials for Compact Motion Systems (MECOMOS), project number 18940 of the Open Technology Program financed by the Dutch Research Council (NWO).

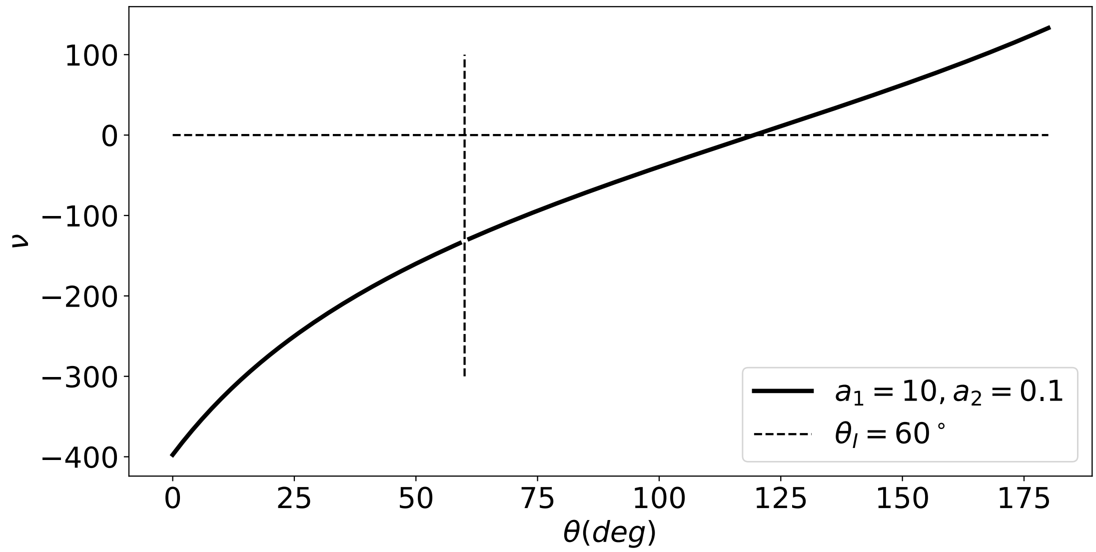

Fig. A.17. Evolution of the Poisson's ratio (ν) of Z with $a_1 = 10$ and $a_2 = 0.1$ (with arbitrary units) from and initial angle $\theta_I = 60°$.

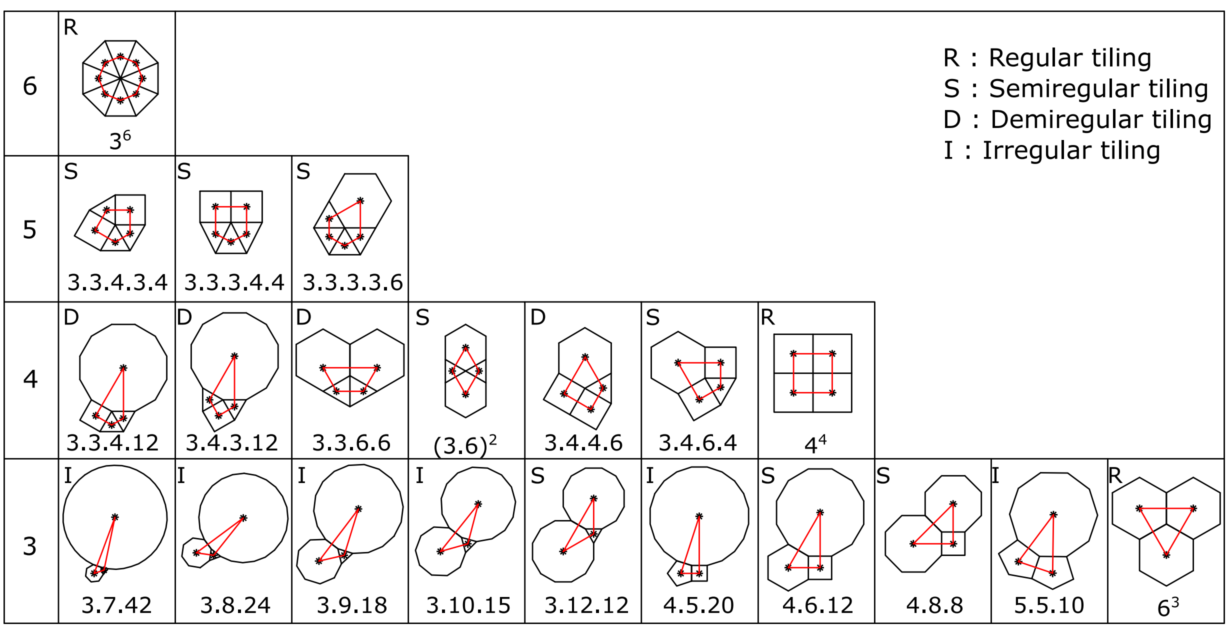

Fig. B.18. Archimedean tiling of the unit cells and Laves tiling with the construction of the planigons (Golomb et al., 1988).

Appendix A. Extreme Poisson's ratio values for Z

See Fig. A.17.

Appendix B. Tessellation of unit cells

The unit cells are usually tessellated in the plane as the repetition of a single type of structure following the Wigner–Seitz tessellation. This tessellation allows the repetition, in the plane, of the unit cells shaped as regular lozenges ($N = 2, 4$) (squares and rectangles) and regular hexagons ($N = 6$), following a translation $\vec{T}$

$$\vec{T} = u_1 \vec{a}_1 + u_2 \vec{a}_2 \tag{B.1}$$

with two unit vectors $\vec{a}_1$ and $\vec{a}_2$, and two integers u_1 and u_2. Identical triangular unit cells ($N = 3$) are to be joined, by one face, to a second triangular cell to form a lozenge to be a tessellable WS cell. The Wigner–Seitz tessellation is limited to regular identical shapes, a more complete tessellation of the plane is defined by the Archimedean tessellation, where the Wigner–Seitz is a particular regular case. The archimedean tiling or plane-vertex tiling (also called semiregular tiling) uses regular convex polygons that can form 21 plane-vertex tilings (Golomb et al., 1988; Yang and Ma, 2018). The 21 plane-vertex tilings or planigons are classified in four families,

1. 3 regular planigons are the equilateral triangles, squares, and regular hexagons;
2. 8 semiregular planigons such as triangles, quadrilaterals, and pentagons;
3. 4 "demiregular" planigons, they can only fill the plane combining other planigons;
4. 6 irregular planigons that can fill the plane only by combining with irregular polygons.

Planigons are tiled edge-to-edge as the angles are divisors of 360° and connect the vertexes together. The tessellation possibilities offered by the Archimedean plane vertex tiling or Laves tiling are detailed in Fig. B.18.

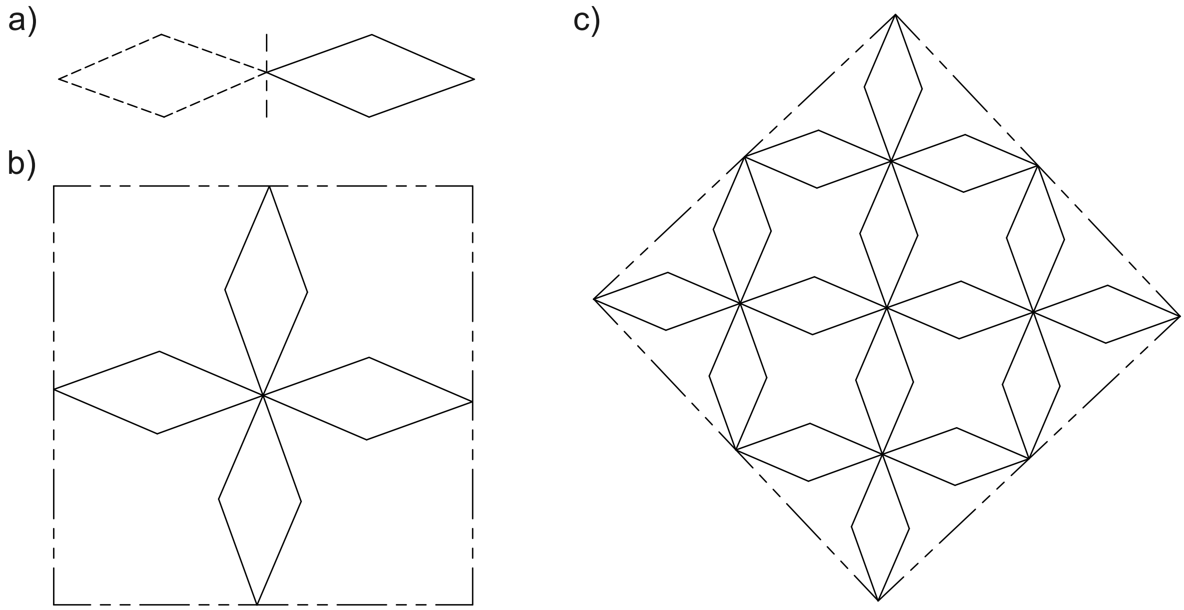

Fig. C.19. Representation of (a) the Sf base structures which is half of the Wr base structure where $a_1 = 0$ and $a_2 = a_3$ (or $a_3 = 0$ and $a_2 = a_1$), (b) the copy-rotated structure $4CSf$ (similar to $4RSf$) which presents an anepirretic behavior because of the center point which decouples the different axis of the structure, and (c) the higher order copy-rotated structure $4.4CSf$ (similar to $4.4RSf$) which should present a meiotic behavior when stretched in the direction normal to the unit cell, and an anepirretic behavior, as $4CSf$, if stretched in the direction of the rhombi.

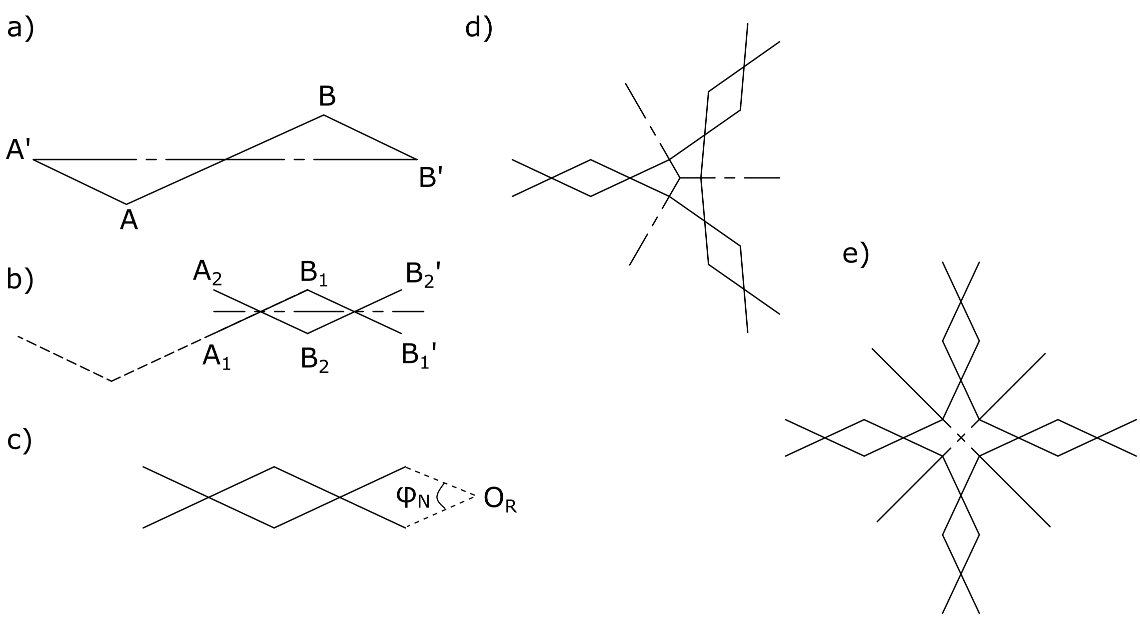

Fig. D.20. Representation of (a) the Wr base structures with its regular axis of symmetry passing through the points A' and B', (b) represents one irregular axis to form the Sm structures, where the axis is parallel to $(A'B')$ and $a_1 = a_2$ and $a_3 = 0$ (or $a_2 = a_3$ and $a_1 = 0$), (c) represents the Scissors mechanism (Sm) with its center of rotation O_R and the angle φ_N, (d) illustrates the case $3CSm$ (which is similar to $3RSm$), and (e) the illustration of the case $4CSm$ (also similar to $4RSm$).

Appendix C. Snowflake (Sf) design

See Fig. C.19.

Appendix D. Scissors mechanism (Sm) design

See Fig. D.20.

Appendix E. Tessellation of Cg and Cgm structures

See Fig. E.21.

Appendix F. Irregular Hcm_I design

See Fig. F.22.

Appendix G. Butterfly (Bt) achiral meiotic design

See Fig. G.23.

Appendix H. Calculation of Poisson's ratio and surface strain

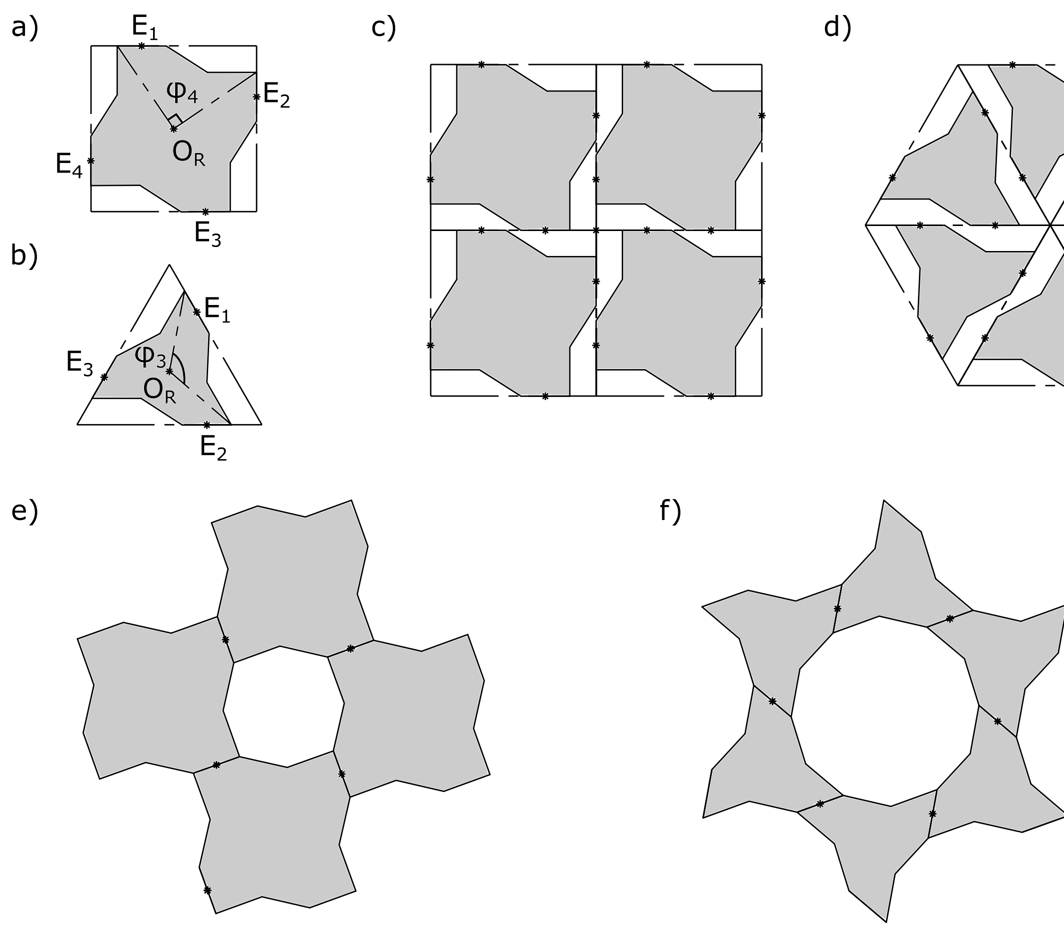

Fig. E.21. Representation of (a) the Hcm irregular (Hcm_I) structure with the length $a_3 = a_1 \neq 0$, the representation of the copy-rotated structures (top) and the unit cell (bottom) of (b) Hcm_I3, and (c) Hcm_I4. (d) Representation of the auxetic structure $Hcm_I4.4$ based on eight rotating squares, in gray, and (e) the representation of the meiotic achiralised structure $2RAHcm_I4$, based on the "Butterfly" (Bt) design, in gray (Appendix G).

The details of the calculation of the length and height of $2Clb$ (Fig. H.24.a) were presented in Section 3.4. Here we present the calculation of three other meiotic structures, $4CLb$, $4RLb$, $2CACgm4$ and $2CAMrm4$, represented in Fig. H.24. The length and height of the structures can be written as a function of the angle α and the length parameters a_1, a_2 and a_3.

The initial dimensions of $4CLb$ (Fig. H.24.a) are dependent on the angle θ_I, if $\theta_I < 90°$ the structure behaves as an auxetic structure and all sectors are behaving similarly with the length

$$L(\theta) = 2\left(a_1 - a_2\cos(\theta) + a_2\sin(\theta)\right) \tag{H.1}$$

and height

$$H(\theta) = 2\left(a_1 + a_2\cos(\theta) - a_2\sin(\theta)\right) \tag{H.2}$$

In the case of $\theta_I > 90°$ the structure becomes meiotic and here we assume that the initial angle normal to the tension or compression is not deformed, otherwise the rate of deformation depends on the stiffness of the revolute joints in the structure. The length becomes

$$L(\theta) = 2\left(a_1 - a_2\cos(\theta) + a_2\sin(\theta_I)\right) \tag{H.3}$$

and height

$$H(\theta) = 2\left(a_1 + a_2\cos(\theta) - a_2\sin(\theta_I)\right) \tag{H.4}$$

The structure $4RLb$ (Fig. H.24.b) possesses similar initial dimensions

$$L(\theta_I) = H(\theta_I) = 2\left(2a_1 + a_2\cos\left(\theta_I\right)\right) \tag{H.5}$$

When stretched, the cross-like rigid body decouples the x and y directions. The length becomes

$$L(\theta) = 2\left(2a_1 + a_2\cos(\theta)\right) \tag{H.6}$$

and the height remains unchanged. As the Poisson's ratio is below 0.5 the surface strain is positive.

The structure $2CACgm4$ (Fig. H.24.c) is, oppositely to $2CAMrm4$ and $2CAHcm4$ non an anisotropic PRM (ani-PRM), unless the axis of achiralisation is tilted. The structure is symmetric and therefore the length and height are similar

$$L(\theta) = H(\theta) = 2\left(a_3 + a_1 - a_2\cos(\theta) + a_2\sin(\theta)\right) \tag{H.7}$$

The structure is meiotic but does not exhibit negative compressibility.

Appendix I. Hierarchical auxetic-meiotic

See Fig. I.25.

Data availability

No data was used for the research described in the article.

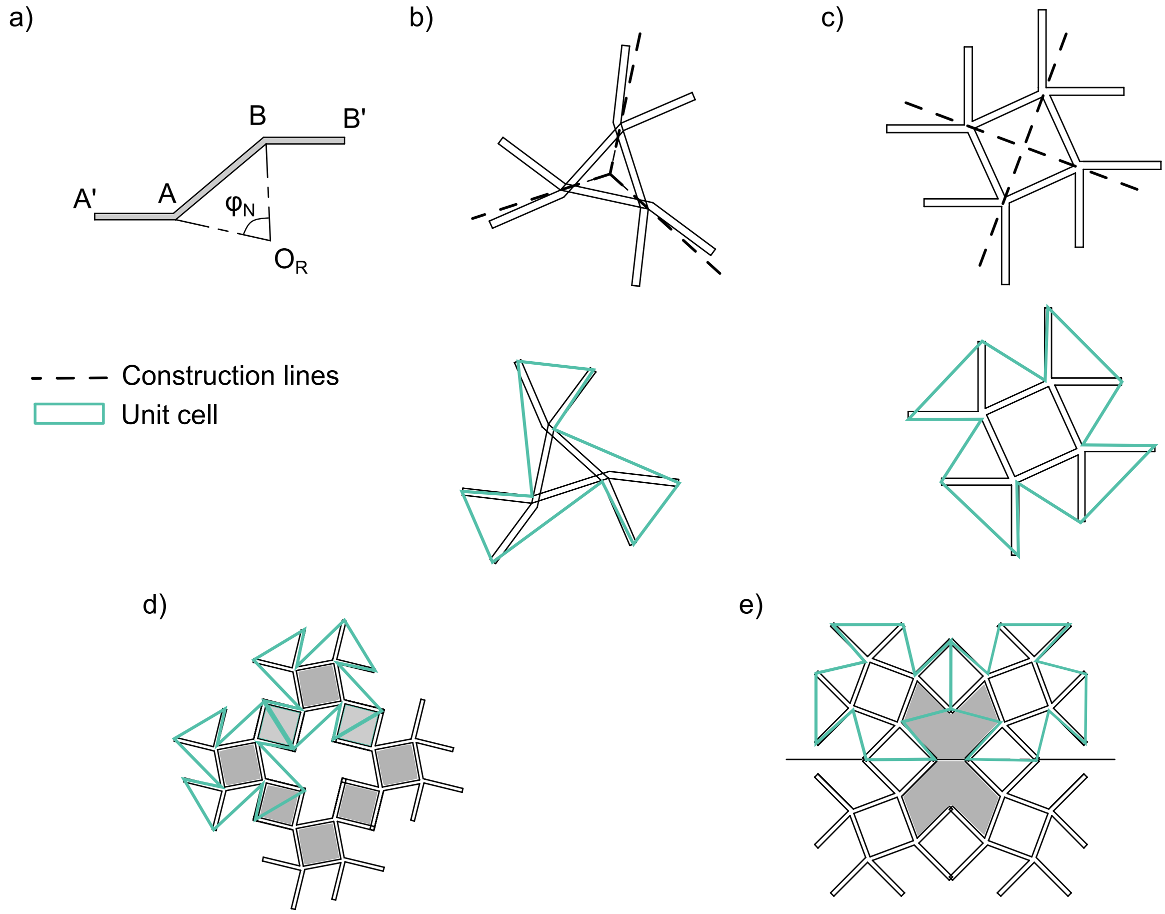

Fig. F.22. Representation of (a) the structure and unit cell of $Cgm4$, and (b) the structure and unit cell of $Cgm3$ with their regular tessellation, connecting (c) the square unit cells and, (d) triangular unit cell respectively, however the regular unit cells are not connecting (the internal surface of the structures are colored in gray for visual clarity). The structures can be connected with their edge points E_N and connecting rigidly the edges and the beams, for (e) $Cgm4$ and, (f) for $Cgm3$.

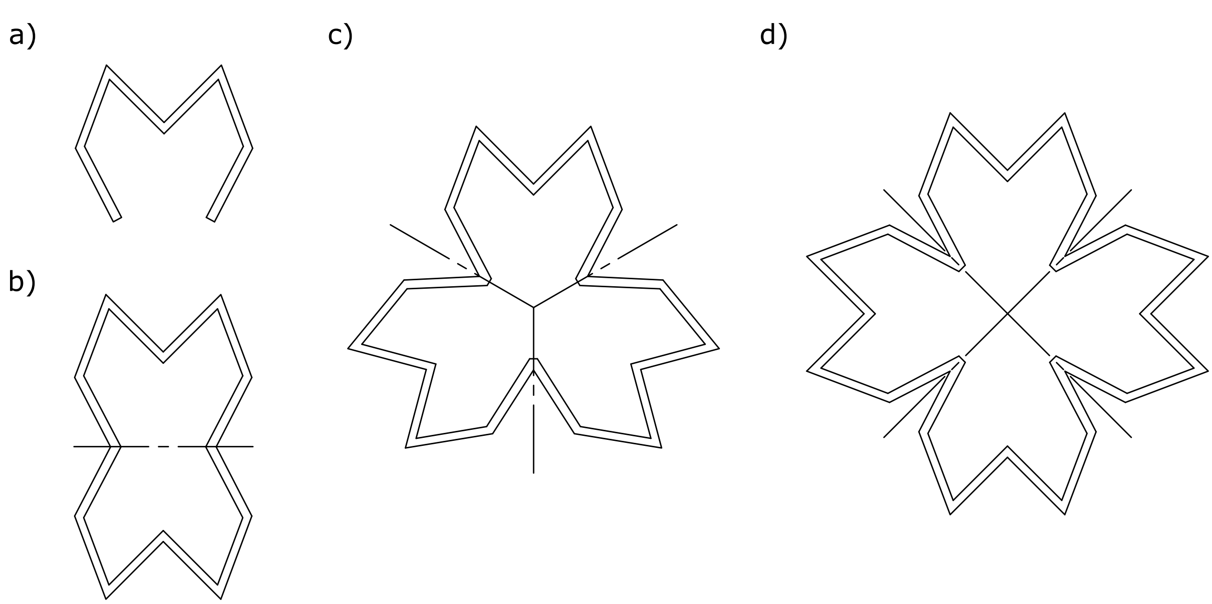

Fig. G.23. Representation of the butterfly Bt (a) base, and the structures (b) $2CBt$, (c) $3CBt$, and (d) $4CBt$.

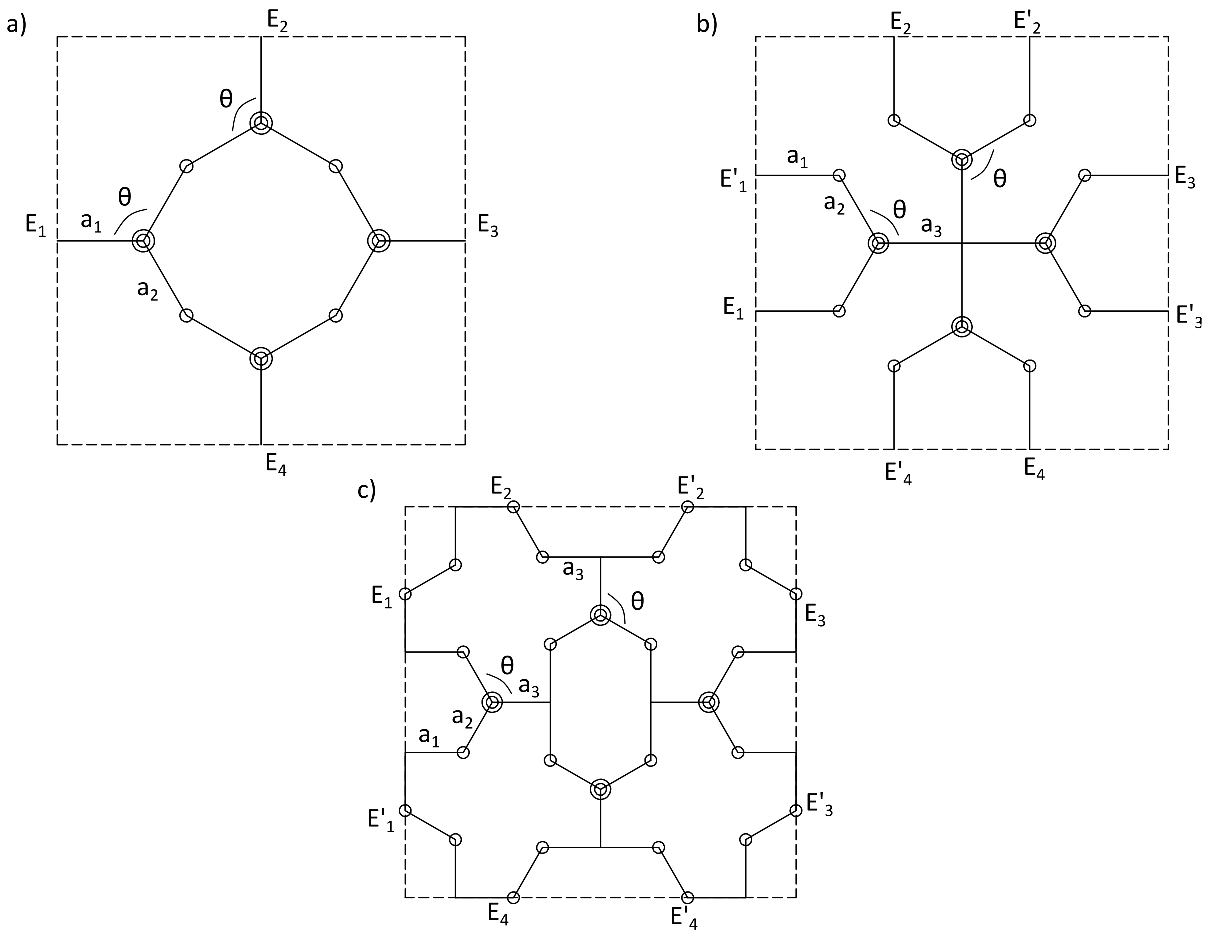

Fig. H.24. Representation of the hierarchical $4.4.2CACgm4$ structure (a) undeployed and (b) partially deployed, with the red dots the selected hinges allowing a larger range of motion (Jalali et al., 2022).

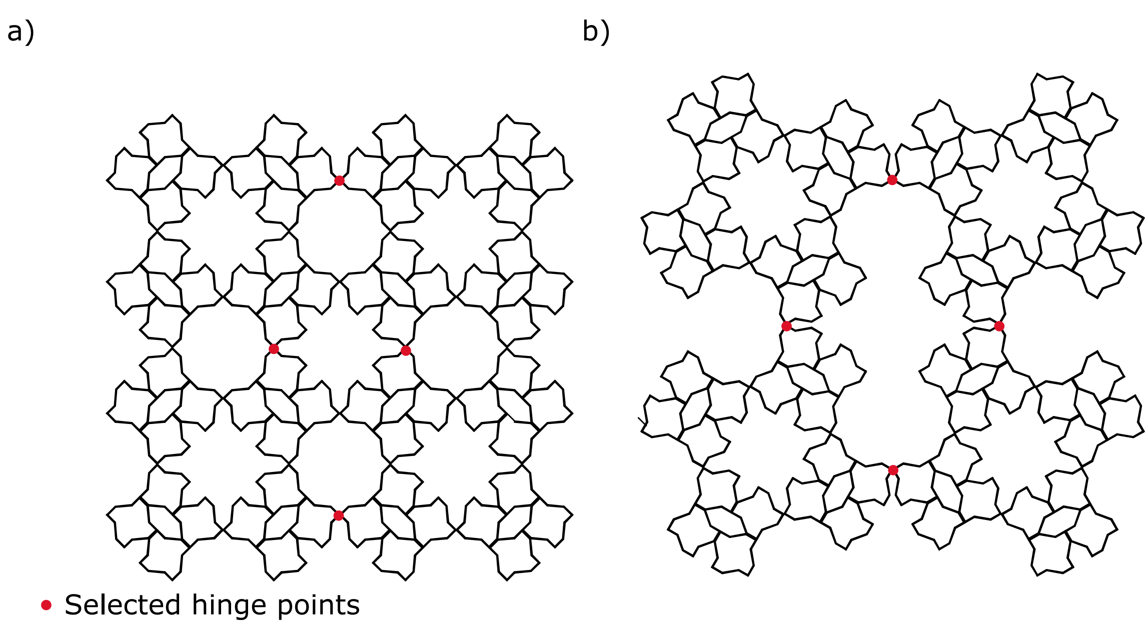

Fig. I.25. Representation of the topology, in their unit cells, of (a) $4CLb$, (b) $4RLb$, (c) $2CACgm4$.

References

Baughman, R.H., Stafström, S., Cui, C., Dantas, S.O., 1998. Materials with negative compressibilities in one or more dimensions. Sci. 279 (5356), 1522–1524. http://dx.doi.org/10.1126/science.279.5356.1522.

Broeren, F.G.J., Herder, J.L., van der Wijk, V., 2019. On the synthesis of periodic linkages with a specific constant Poisson's ratio. In: Uhl, T. (Ed.), Advances in Mechanism and Machine Science. In: Mechanisms and Machine Science, Springer International Publishing, Cham, pp. 249–257. http://dx.doi.org/10.1007/978-3-030-20131-9_25.

Broeren, F.G., van der Wijk, V., Herder, J.L., 2020. Spatial pseudo-rigid body model for the analysis of a tubular mechanical metamaterial. Math. Mech. Solids 25 (2), 305–316. http://dx.doi.org/10.1177/1081286519875500.

Cairns, A.B., Catafesta, J., Levelut, C., Rouquette, J., van der Lee, A., Peters, L., Thompson, A.L., Dmitriev, V., Haines, J., Goodwin, A.L., 2013. Giant negative linear compressibility in zinc dicyanoaurate. Nat. Mater. 12 (3), 212–216. http://dx.doi.org/10.1038/nmat3551.

Chamis, C.C., 1980. Prediction of Fiber Composite Mechanical Behavior Made Simple. New Orleans, URL: https://ntrs.nasa.gov/citations/19800007847.

Clausen, A., Wang, F., Jensen, J.S., Sigmund, O., Lewis, J.A., 2015. Topology optimized architectures with programmable Poisson's ratio over large deformations. Adv. Mater. 27 (37), 5523–5527. http://dx.doi.org/10.1002/adma.201502485.

Czajkowski, M., Coulais, C., van Hecke, M., Rocklin, D.Z., 2022. Conformal elasticity of mechanism-based metamaterials. Nat. Commun. 13 (1), 211. http://dx.doi.org/10.1038/s41467-021-27825-0.

Dagdelen, J., Montoya, J., de Jong, M., Persson, K., 2017. Computational prediction of new auxetic materials. Nat. Commun. 8 (1), 323. http://dx.doi.org/10.1038/s41467-017-00399-6.

dell'Isola, F., Lekszycki, T., Pawlikowski, M., Grygoruk, R., Greco, L., 2015. Designing a light fabric metamaterial being highly macroscopically tough under directional extension: first experimental evidence. Z. Angew. Math. Phys. 66 (6), 3473–3498. http://dx.doi.org/10.1007/s00033-015-0556-4.

dell'Isola, F., Seppecher, P., Spagnuolo, M., Barchiesi, E., Hild, F., Lekszycki, T., Giorgio, I., Placidi, L., Andreaus, U., Cuomo, M., Eugster, S.R., Pfaff, A., Hoschke, K., Langkemper, R., Turco, E., Sarikaya, R., Misra, A., De Angelo, M., D'Annibale, F., Bouterf, A., Pinelli, X., Misra, A., Desmorat, B., Pawlikowski, M., Dupuy, C., Scerrato, D., Peyre, P., Laudato, M., Manzari, L., Göransson, P., Hesch, C., Hesch, S., Franciosi, P., Dirrenberger, J., Maurin, F., Vangelatos, Z., Grigoropoulos, C., Melissinaki, V., Farsari, M., Muller, W., Abali, B.E., Liebold, C., Ganzosch, G., Harrison, P., Drobnicki, R., Igumnov, L., Alzahrani, F., Hayat, T., 2019. Advances in pantographic structures: design, manufacturing, models, experiments and image analyses. Contin. Mech. Thermodyn. 31 (4), 1231–1282. http://dx.doi.org/10.1007/s00161-019-00806-x.

Dirrenberger, J., Forest, S., Jeulin, D., Colin, C., 2011. Homogenization of periodic auxetic materials. Procedia Eng. 10, 1847–1852. http://dx.doi.org/10.1016/j.proeng.2011.04.307.

Dudek, K.K., Attard, D., Caruana-Gauci, R., Wojciechowski, K.W., Grima, J.N., 2016. Unimode metamaterials exhibiting negative linear compressibility and negative thermal expansion. Smart Mater. Struct. 25 (2), 025009. http://dx.doi.org/10.1088/0964-1726/25/2/025009.

Fortes, A.D., Suard, E., Knight, K.S., 2011. Negative linear compressibility and massive anisotropic thermal expansion in methanol monohydrate. Sci. 331 (6018), 742–746. http://dx.doi.org/10.1126/science.1198640.

Fortes, M.A., Teresa Nogueira, M., 1989. The poison effect in cork. Mater. Sci. Eng.: A 122 (2), 227–232. http://dx.doi.org/10.1016/0921-5093(89)90634-5.

Frolich, L.M., LaBarbera, M., Stevens, W.P., 1994. Poisson's ratio of a crossed fibre sheath: the skin of aquatic salamanders. J. Zool. 232 (2), 231–252. http://dx.doi.org/10.1111/j.1469-7998.1994.tb01571.x.

Gatt, R., Grima, J.N., 2008. Negative compressibility. Phys. Status Solidi (RRL) – Rapid Res. Lett. (5), 236–238. http://dx.doi.org/10.1002/pssr.200802101.

Gatt, R., Mizzi, L., Azzopardi, J.I., Azzopardi, K.M., Attard, D., Casha, A., Briffa, J., Grima, J.N., 2015a. Hierarchical auxetic mechanical metamaterials. Sci. Rep. 5 (1), 8395. http://dx.doi.org/10.1038/srep08395.

Gatt, R., Vella Wood, M., Gatt, A., Zarb, F., Formosa, C., Azzopardi, K.M., Casha, A., Agius, T.P., Schembri-Wismayer, P., Attard, L., Chockalingam, N., Grima, J.N., 2015b. Negative Poisson's ratios in tendons: An unexpected mechanical response. Acta Biomater. 24, 201–208. http://dx.doi.org/10.1016/j.actbio.2015.06.018.

Giraud, F.H., Mete, M., Paik, J., 2022. Flexure variable stiffness actuators. Adv. Intell. Syst. 4 (7), 2100282. http://dx.doi.org/10.1002/aisy.202100282.

Golomb, S.W., Grunbaum, B., Shephard, G.C., 1988. Tilings and patterns. In: The American Mathematical Monthly. Vol. 95, p. 63. http://dx.doi.org/10.2307/2323457.

Grima, J.N., Attard, D., Caruana-Gauci, R., Gatt, R., 2011. Negative linear compressibility of hexagonal honeycombs and related systems. Scr. Mater. 65 (7), 565–568. http://dx.doi.org/10.1016/j.scriptamat.2011.06.011.

Grima, J.N., Attard, D., Gatt, R., 2008. Truss-type systems exhibiting negative compressibility. Phys. Status Solidi (B) 245 (11), 2405–2414. http://dx.doi.org/10.1002/pssb.200880267.

Grima, J.N., Gatt, R., Alderson, A., Evans, K.E., 2005. On the potential of connected stars as auxetic systems. Mol. Simul. 31 (13), 925–935. http://dx.doi.org/10.1080/08927020500401139.

Hamzehei, R., Kadkhodapour, J., Anaraki, A.P., Rezaei, S., Dariushi, S., Rezadoust, A.M., 2018. Octagonal auxetic metamaterials with hyperelastic properties for large compressive deformation. Int. J. Mech. Sci. 145, 96–105. http://dx.doi.org/10.1016/j.ijmecsci.2018.06.040.

Hamzehei, R., Serjouei, A., Wu, N., Zolfagharian, A., Bodaghi, M., 2022. 4D metamaterials with zero Poisson's ratio, shape recovery, and energy absorption features. Adv. Eng. Mater. 24 (9), 2200656. http://dx.doi.org/10.1002/adem.202200656.

Jalali, E., Soltanizadeh, H., Chen, Y., Xie, Y.M., Sareh, P., 2022. Selective hinge removal strategy for architecting hierarchical auxetic metamaterials. Commun. Mater. 3 (1), 1–15. http://dx.doi.org/10.1038/s43246-022-00322-7.

Kang, L., Jiang, X., Luo, S., Gong, P., Li, W., Wu, X., Li, Y., Li, X., Chen, C., Lin, Z., 2015. Negative linear compressibility in a crystal of α-BiB3O6. Sci. Rep. 5 (1), 13432. http://dx.doi.org/10.1038/srep13432.

Kolken, H.M., Zadpoor, A., 2017. Auxetic mechanical metamaterials. RSC Adv. 7 (9), 5111–5129. http://dx.doi.org/10.1039/C6RA27333E.

Kolpakov, A.G., 1985. Determination of the average characteristics of elastic frameworks. J. Appl. Math. Mech. 49 (6), 739–745. http://dx.doi.org/10.1016/0021-8928(85)90011-5.

Lakes, R., 1987. Foam structures with a negative Poisson's ratio. Sci. (N. Y. N. Y.) 235 (4792), 1038–1040. http://dx.doi.org/10.1126/science.235.4792.1038.

Lakes, R., Wojciechowski, K.W., 2008. Negative compressibility, negative Poisson's ratio, and stability. Phys. Status Solidi (B) 245 (3), 545–551. http://dx.doi.org/10.1002/pssb.200777708.

Li, X., Fan, R., Fan, Z., Lu, Y., 2021. Programmable mechanical metamaterials based on hierarchical rotating structures. Int. J. Solids Struct. 216, 145–155. http://dx.doi.org/10.1016/j.ijsolstr.2021.01.028.

Li, X., Wang, Q., Yang, Z., Lu, Z., 2019. Novel auxetic structures with enhanced mechanical properties. Extrem. Mech. Lett. 27, 59–65. http://dx.doi.org/10.1016/j.eml.2019.01.002.

Lim, T.-C., 2020. Negative compressibility. In: Lim, T.-C. (Ed.), Mechanics of Metamaterials with Negative Parameters. In: Engineering Materials, Springer, Singapore, pp. 427–463. http://dx.doi.org/10.1007/978-981-15-6446-8_12.

Magos-Palasyuk, E., Fijalkowski, K.J., Palasyuk, T., 2016. Chemically driven negative linear compressibility in sodium amidoborane, Na(NH2BH3). Sci. Rep. 6 (1), 28745. http://dx.doi.org/10.1038/srep28745.

Mandelbrot, B.B., 1983. The Fractal Geometry of Nature. Henry Holt and Company.

Nicolaou, Z.G., Motter, A.E., 2012. Mechanical metamaterials with negative compressibility transitions. Nat. Mater. 11 (7), 608–613. http://dx.doi.org/10.1038/nmat3331.

Overvelde, J.T.B., de Jong, T.A., Shevchenko, Y., Becerra, S.A., Whitesides, G.M., Weaver, J.C., Hoberman, C., Bertoldi, K., 2016. A three-dimensional actuated origami-inspired transformable metamaterial with multiple degrees of freedom. Nat. Commun. 7 (1), 10929. http://dx.doi.org/10.1038/ncomms10929.

Overvelde, J.T.B., Weaver, J.C., Hoberman, C., Bertoldi, K., 2017. Rational design of reconfigurable prismatic architected materials. Nat. 541 (7637), 347–352. http://dx.doi.org/10.1038/nature20824.

Papadopoulou, A., Laucks, J., Tibbits, S., 2017. Auxetic materials in design and architecture. Nat. Rev. Mater. 2 (12), 1–3. http://dx.doi.org/10.1038/natrevmats.2017.78.

Roberjot, P., Herder, J.L., 2024. A unified design method for 2D auxetic metamaterials based on a minimal auxetic structure. Int. J. Solids Struct. 295, 112777. http://dx.doi.org/10.1016/j.ijsolstr.2024.112777.

Shaat, M., Wagih, A., 2020. Hinged-3D metamaterials with giant and strain-independent Poisson's ratios. Sci. Rep. 10 (1), 2228. http://dx.doi.org/10.1038/s41598-020-59205-x.

Silverberg, J.L., Na, J.-H., Evans, A.A., Liu, B., Hull, T.C., Santangelo, C.D., Lang, R.J., Hayward, R.C., Cohen, I., 2015. Origami structures with a critical transition to bistability arising from hidden degrees of freedom. Nat. Mater. 14 (4), 389–393. http://dx.doi.org/10.1038/nmat4232.

Turco, E., dell'Isola, F., Rizzi, N.L., Grygoruk, R., Müller, W.H., Liebold, C., 2016. Fiber rupture in sheared planar pantographic sheets: Numerical and experimental evidence. Mech. Res. Commun. 76, 86–90. http://dx.doi.org/10.1016/j.mechrescom.2016.07.007.

Turco, E., Rizzi, N.L., 2016. Pantographic structures presenting statistically distributed defects: Numerical investigations of the effects on deformation fields. Mech. Res. Commun. 77, 65–69. http://dx.doi.org/10.1016/j.mechrescom.2016.09.006.

Wang, D., Dong, L., Gu, G., 2022. 3D printed fractal metamaterials with tunable mechanical properties and shape reconfiguration. Adv. Funct. Mater. 33, http://dx.doi.org/10.1002/adfm.202208849.

Wang, H., Feng, M., Wang, Y.-F., Gu, Z.-Y., 2016. H3O+ tetrahedron induction in large negative linear compressibility. Sci. Rep. 6 (1), 26015. http://dx.doi.org/10.1038/srep26015.

Williams, J.L., Lewis, J.L., 1982. Properties and an anisotropic model of cancellous bone from the proximal tibial epiphysis. J. Biomech. Eng. 104 (1), 50–56. http://dx.doi.org/10.1115/1.3138303.

Yang, H., Ma, L., 2018. Multi-stable mechanical metamaterials with shape-reconfiguration and zero Poisson's ratio. Mater. Des. 152, 181–190. http://dx.doi.org/10.1016/j.matdes.2018.04.064.

Zhang, Y., Ren, X., Jiang, W., Han, D., Yu Zhang, X., Pan, Y., Min Xie, Y., 2022. In-plane compressive properties of assembled auxetic chiral honeycomb composed of slotted wave plate. Mater. Des. 221, 110956. http://dx.doi.org/10.1016/j.matdes.2022.110956.

Zhang, Y.-J., Wang, L.-C., Song, W.-L., Chen, M., Fang, D., 2020. Hexagon-twist frequency reconfigurable antennas via multi-material printed thermo-responsive origami structures. Front. Mater. 7, http://dx.doi.org/10.3389/fmats.2020.600863.

Zhu, Y., Fei, F., Fan, S., Cao, L., Donda, K., Assouar, B., 2019. Reconfigurable origami-inspired metamaterials for controllable sound manipulation. Phys. Rev. Appl. 12 (3), 034029. http://dx.doi.org/10.1103/PhysRevApplied.12.034029.

Zhu, Y., Jiang, S., Lu, F., Ren, X., 2022. A novel enhanced anti-tetra-missing rib auxetic structure with tailorable in-plane mechanical properties. Eng. Struct. 262, 114399. http://dx.doi.org/10.1016/j.engstruct.2022.114399.